
Article:
Bjorkman, M.P., Vega, C.P., Kuhnel, R. et al. (8 more authors) (2014) Nitrate postdeposition processes in Svalbard surface snow. Journal of Geophysical Research, 119 (22). 12,953-12,976. ISSN 0148-0227

https://doi.org/10.1002/2013JD021234

Manuscript to: *Journal of Geophysical Research*

Text pages: 44 Tables: 3 Figures: 7

Title: **Nitrate post-depositional processes in Svalbard surface snow**

Authors: Mats P. Björkman[1,2,3*], Carmen P. Vega[4], Rafael Kühnel[1,2], Francesca Spataro[5], Antonietta Ianniello[5], Giulio Esposito[5], Jan Kaiser[6], Alina Marca[6], Andy Hodson[7], Elisabeth Isaksson[1] and Tjarda J. Roberts[8]

[1]Norwegian Polar Institute, Fram Centre, N-9296 Tromsø, Norway.

[2]Department of Geosciences, University of Oslo, P.O. Box 1047 Blindern, 0316 Oslo, Norway.

[3]Now at: Department of Earth Sciences, University of Gothenburg, Box 460, SE-40530 Göteborg, Sweden.

[4]Department of Earth Sciences, Uppsala University, Villavägen 16, SE-76236, Uppsala, Sweden.

[5]C.N.R.-Istituto sull'Inquinamento Atmosferico (IIA), Via Salaria Km 29.300, I-00015 Monterotondo Scalo (Roma), Italy.

[6]School of Environmental Sciences, University of East Anglia, Norwich NR4 7TJ, U.K.

[7]Department of Geography, University of Sheffield, Sheffield S10 2TN, U.K.

[8]LPC2E, UMR 7328, CNRS-Université d'Orléans, 3A avenue de la Recherche Scientifique, 45071 Orléans, Cedex 2, France.

[*]**Corresponding author**

Mats P. Björkman, Department of Earth Sciences, University of Gothenburg, Box 460, SE-40530 Göteborg, Sweden.

E-mail: mats.p.bjorkman@gmail.com

Telephone number: +46 (0) 730581145

Key points

- NO_3^- deposition and snowpack processes quantified by surface snow sampling
- NO_3^- dry deposition dominates over post-dep. loss in Ny-Ålesund surface snow.
- Br^- decreases whilst NO_3^- $d(^{18}O)$ increases, suggesting tied BrO-NO_x chemistry

Abstract

The snowpack acts as a sink for atmospheric reactive nitrogen, but several post-depositional pathways have been reported to alter the concentration and isotopic composition of snow nitrate with implications for atmospheric boundary layer chemistry, ice core records and terrestrial ecology following snow-melt. Careful daily sampling of surface snow during winter (11 – 15 February, 2010) and spring-time (April 9 – May 5, 2010) near Ny-Ålesund, Svalbard reveals a complex pattern of processes within the snowpack. Dry deposition was found to dominate over post-depositional losses, with a net nitrate deposition rate of (0.6±0.2) μmol m^{-2} d^{-1} to homogeneous surface snow. At Ny-Ålesund, such surface dry deposition can either solely result from long-range atmospheric transport of $NO_{x,y}$ or include the re-deposition of photolytic/bacterial emission originating from deeper snow layers. Our data further confirm that polar basin air masses bring ^{15}N-depleted nitrate to Svalbard, while high nitrate $\delta(^{18}O)$ values only occur in connection with ozone-depleted air, and show that these signatures are reflected in the deposited nitrate. Such ozone-depleted air is attributed to active halogen chemistry in the air-masses advected to the site. However, here the Ny-Ålesund surface snow was shown to have an

active role in the halogen dynamics for this region, as indicated by declining bromide concentrations and increasing nitrate $\delta(^{18}O)$, during high BrO (low ozone) events. The data also indicates that the snow-pack BrO-NO_x cycling continued in post-event periods, when ambient ozone and BrO levels recovered.

1. Introduction

1.1 Overview

Snowpack nitrate (NO_3^-) can influence the chemical composition of the lower atmospheric boundary layer through photochemical release of nitrogen oxides (e.g. Honrath et al., 1999, Domine and Shepson, 2002; Grannas et al., 2007; Morin et al., 2009; Thomas et al., 2012). Even though snow is a highly reflective material, the shape and small size of snow grains favours a forward scattering of the light into the snowpack (Domine et al., 2008), creating a photo-active zone in the surface region of the snow cover (e.g. Qiu et al., 2002; Simpson et al., 2002; Galbavy et al., 2007). Following polar sunrise, photolysis of surface snow NO_3^- and the concomitant emission of nitric oxide (NO) and nitrogen dioxide (NO_2) can alter the isotopic composition and concentration of NO_3^- in snow and ice (Jarvis et al., 2008; Frey et al., 2009; Erbland et al., 2013). Furthermore, the removal of NO_3^- through HNO_3 evaporation from snow can also contribute to NO_3^- isotopic and concentration changes (Frey et al., 2009; Erbland et al., 2013). In addition to these post-depositional processes, dry deposition of pollutants and further accumulation of snow will influence the isotopic composition and budget of NO_3^-, where the snow accumulation buries older layers and prevents further photolytic reactions (Jarvis et al., 2009; Erbland et al., 2013). Since several pathways have been described for the NO_x (NO_x = NO + NO_2) oxidation to nitric acid (HNO_3) in polar regions, e.g. involving ozone (O_3), hydroxyl (OH) and bromine monoxide (BrO) species (Russell et al., 1985; Evans et al., 2003; Seinfeld and Pandis, 2006; Morin et al.,

69 2007b), atmospheric boundary layer chemistry is of key importance for the isotopic NO_3^-
70 signature found in snow.

71 Here we present a detailed investigation of the processes governing the concentration and
72 isotopic composition of NO_3^- ($^{15}N/^{14}N$ and $^{18}O/^{16}O$) in the most photo-active zone (upper 5 cm)
73 of the snowpack at Ny-Ålesund, Svalbard (Fig. 1). In order to highlight the effects of photolysis,
74 the sampling period covered both the polar night and springtime during 2010. The data was
75 analyzed in conjunction with atmospheric flux measurements of oxidized nitrogen; NO, NO_2,
76 HNO_3 and particulate NO_3^- (p-NO_3^-), that were conducted directly above the snowpack, and O_3
77 concentrations monitored both at Gruvebadet and at the nearby Zeppelin Station (Fig. 1). This
78 study is used to infer the influence of BrO chemistry upon the snowpack nitrogen cycle for the
79 first time in Svalbard.

80 1.2 Background

81 1.2.1 Long-range transport and deposition of oxidized nitrogen

82 Through *long-range atmospheric transport* (Fig. 2) oxidized nitrogen that is emitted at mid-
83 latitude regions can reach pristine Arctic environments (Rahn et al., 1980; Rahn, 1981;
84 Dickerson, 1985; Stohl, 2006; Hirdman et al., 2010; Kühnel et al., 2011; Kühnel, 2013), often in
85 the form of molecules with longer atmospheric residence time such as peroxyacyl nitrates
86 (PANs) or p-NO_3^- (Beine et al., 1997; Seinfeld and Pandis, 2006). However, occasional rapid
87 long-range transport events also occur, as recently identifed for Ny-Ålesund in the European
88 high Arctic (e.g. Hodson et al., 2010, Kühnel 2013), which can transport pollutants with shorter
89 life-times, such as NO_x, (or its oxidation product HNO_3) into the Arctic (Zien et al., 2014). The
90 original isotopic composition of each NO_x source (e.g. forest fires or fossil fuel combustion,
91 among other) depends on the oxidation process and origin of the nitrogen (N) and oxygen (O)

92 (e.g. Kendall et al., 2007). In the Arctic spring, the long-range transported oxidized nitrogen
93 pollutants, such as PANs, decompose and undergo local boundary layer *NO_x-cycling*, involving
94 O_3, BrO or hydroperoxyl radicals (HO_2) and solar radiation (*hv*, Fig. 2). This cycling is followed
95 by a *NO_x-removal*, where both a day time (through OH or HO_2) and a night time (through NO_3
96 and dinitrogen pentoxide (N_2O_5)) conversion of NO_2 to HNO_3 occurs (Fig. 2, Russell et al.,
97 1985; Dentener and Crutzen, 1993; Hanson and Ravishankara, 1995; Hanson et al., 1996; Evans
98 et al., 2003; Morin et al., 2007b; Morin et al., 2008; Thomas et al., 2011; Thomas et al., 2012),
99 where the N_2O_5 also can be directly deposited to the snow (e.g. Huff et al., 2011). For Arctic
100 sites, HNO_3 production via the *BrO-pathway*, involving $BrONO_2$ (Fig. 2), is particularly
101 important during episodes of BrO chemistry, which also causes low O_3 levels (e.g. Evans et al.,
102 2003; Morin et al., 2007b). Nitric acid and p-NO_3^- will then be removed from the atmosphere by
103 snow, rain or dry deposition (Cadle, 1991; Bergin et al., 1995; Kuhn, 2001), and be deposited to
104 the snow as NO_3^- (Diehl et al., 1995; Abbatt, 1997). The snowpack therefore acts as an important
105 sink and reservoir for atmospheric reactive nitrogen, with a unique isotopic NO_3^- composition
106 and concentration for each snow layer. For the N-isotopic composition, the *initial* snow signature
107 typically resemble the original source of NO_x, this since the fractionation during NO_x-cycling
108 and removal is considered to be low (Freyer, 1991). For the O-isotopes, the interaction and O-
109 exchange with O_3, BrO, and OH during the NO_x-cycling and NO_x-removal will strongly
110 influence the initial snow O-signature, typically masking any other processes or original source
111 signatures (e.g. Michalski et al., 2003; Jarvis et al., 2009; Morin et al., 2009). Thus the *initial* O-
112 signature provides insights into the oxidation processes that have occurred prior to deposition.
113 These initial concentrations and isotopic imprints may, however, be altered by post-depositional
114 snow processes as will be further outlined below (1.2.2.).

In Svalbard, the NO_3^- deposition and thereby the snow concentration is governed by wet deposition, where a few sporadic "strong" events dominate the total annual deposition (Kühnel et al., 2011). These "strong" deposition events are due to rapid transport of polluted European air masses (e.g. Hodson et al., 2010), which are occasionally channelled northward between a blocking anticyclone, situated over Scandinavia and Central Europe, and an incoming cyclone over the Atlantic (Kühnel, 2013). The typical transport time for such events are about 2 to 5 days and where the air-masses picks up in speed and humidity just prior to the arrival to Svalbard (Kühnel 2013). The estimated winter dry deposition of NO_3^- in this region is modest (approx. 14 %, Björkman et al., 2013), but nevertheless, of importance for the isotopic composition of NO_3^- in snow when studying short term daily variations (Hastings et al., 2004).

1.2.2 Snowpack NO_3^- photolysis and evaporation

Due to NO_x release from the photo-active zone of the snowpack, the deposited NO_3^- can play an important role in atmospheric boundary layer chemistry after the initial deposition (e.g. Thomas et al., 2012). The snowpack is therefore an active player in atmospheric chemical processes and not just a NO_3^- sink (Honrath et al., 1999). Snowpack NO_3^- photolysis, of relevance for the NO_3^- budget, is believed to occur at the very surface of snow crystals (Boxe and Saiz-Lopez, 2008), with reaction rates and quantum yields for photolytic processes similar to those in aqueous solutions (Bartels-Rausch et al., 2014). This region of the ice crystal has previously been referred to as a quasi-liquid layer (QLL, Kvlividz et al., 1970), but has lately been re-described as a disordered interface (DI, Bartels-Rausch et al., 2014). This new term emphasizes the disordered molecular structure that occurs at the surface of any crystal, created by the absence of molecular bonds towards its surface (Bartels-Rausch et al., 2014), instead of involving a liquid state analogy. The photolysis of NO_3^- within the DI and subsequent reactions

(Fig. 2) lead to the production of NO_2 and to a lesser extent NO (see Jacobi and Hilker, 2007; Boxe and Saiz-Lopez, 2008 for an overview of reaction pathways). The produced NO_2 and NO can then diffuse out of the DI into firn air and thereafter into the atmospheric boundary layer (e.g. Honrath et al., 1999; Jones et al., 2000; Beine et al., 2003). This photolytic initiated loss also alters the isotopic composition of snowpack NO_3^-, with an enrichment of ^{15}N in the residual NO_3^- due to photolytic fractionation (Frey et al., 2009; Morin et al., 2009; Erbland et al., 2013). On the other hand the O-composition of the remaining NO_3^- will be strongly influenced by the isotopic exchange between the photolytic products and OH-radical or H_2O within the DI (McCabe et al., 2005; Frey et al., 2009). There is also evidence for nitrous acid (HONO) production from irradiated snow (Fig. 2, Zhou et al., 2001; Beine et al., 2002a), due to the interaction between nitrite (NO_2^-) and a hydrogen ion (H^+, e.g. Dominé and Shepson, 2002). However, several other pathways have also been described; i.e. involving humic acids (e.g. Beine et al., 2008, Villena et al., 2001) or heterogeneous reactions in the firn (e.g. Jacobi and Hilker, 2007), although the reaction steps in these pathways are not fully understood (Grannas et al., 2007; Jacobi and Hilker, 2007; Beine et al., 2008; Boxe and Saiz-Lopez, 2008, Jacobi et al., 2014) and therefore not included in Fig. 2. Nitrate loss from the snow has also been found to be due to *evaporation* (Fig. 2) of HNO_3, a process also favouring the loss of isotopically light NO_3^- (e.g. Frey et al., 2009). A recent study by Erbland et al. (2013) confirms that evaporation is an active player in post-depositional processes in areas with low snow accumulation rates and high firn air ventilation, such as central Antarctic sites. However, the process has been shown to be quantitatively modest compared to the loss through photolysis for these Antarctic sites (Erbland et al., 2013). Interestingly, laboratory studies of snow and ice have found no evidence for this evaporative pathway (Chu and Anastasio, 2003; Sato et al., 2008).

Snowpack NO_x emissions, according to the above post-depositional processes, have been estimated for Arctic, Antarctic and mid-latitude snow (Dibb et al., 1998; Honrath et al., 1999; Honrath et al., 2000; Jones et al., 2000; Jones et al., 2001; Beine et al., 2002a). However, these studies are not necessarily directly applicable to the snowpack in Ny-Ålesund, Svalbard (European high Arctic), where substantially lower snowpack NO_x, HNO_3, p-NO_3^- and HONO emissions have been reported in comparison to the other investigated regions (Beine et al., 2003; Amoroso et al., 2006; Amoroso et al., 2010).

1.2.3 Local biogeochemical contribution to snowpack NO_3^-

The DI reactions described above mostly involve NO_3^- of non-local origin, deposited following long-range atmospheric transport. However, a more locally produced source of oxidized nitrogen has been suggested through microbial activity (Brooks et al., 1997; Ma et al., 2007; Miteva, 2008; Siciliano et al., 2009, Roberts et al., 2010). Svalbard snow is known to contain a diverse community of microorganisms (Amato et al., 2007; Larose et al., 2010), and the microbial assimilation of ammonium (NH_4^+) might result in the production of gas phase NO, HNO_3 and HONO, even during winter (Fig. 2, Amoroso et al., 2010). Isotopic fractionation is expected through microbial assimilation of nitrogen compounds (e.g. Kendall, 1998), although during the nutrient limited conditions in a snowpack such nitrogen isotopic fractionation might not necessarily be expressed in the produced reactive nitrogen emissions (Amoroso et al., 2010). The resulting snowpack emission, under these conditions, would have an N-isotopic composition related to the N source (in this case, organic or mineral bound NH_4^+) and an O-isotopic composition influenced by the surrounding water (Amoroso et al., 2010).

1.2.4 Re-cycling of NO_x snowpack emissions

183 The gas phase products of post-depositional and biogeochemical processes are emitted
184 into the firn air and onwards to the lower atmospheric boundary layer, where further reactions
185 may lead to a re-deposition of HNO_3 to the snow (Fig. 2, Hastings et al., 2004; Morin et al.,
186 2007b; Jarvis et al., 2009). During spring and summer conditions, these reactions can have a
187 diurnal pattern governed by day-time emissions and night-time deposition (Hastings et al., 2004).
188 The isotopic composition of this re-deposited HNO_3 would then be influenced by the oxidation
189 pathways undertaken, see Fig. 2 (e.g. Jarvis et al., 2009). Additionally, snow is a highly porous
190 medium that undergoes a steady exchange of air with the surrounding atmosphere (Sturm and
191 Johnson, 1991; Albert and Hardy, 1995; Colbeck, 1997; Albert et al., 2002; Frey et al., 2005).
192 This exchange allows the boundary layer processes in Fig. 2 to occur also within the snowpack
193 interstitial air pockets.

194 2. Methods

195 2.1 Field sampling

196 The top 5 cm of the snowpack was sampled close to Gruvebadet, 1 km outside the *Ny-*
197 *Ålesund International Arctic Research and Monitoring Facility* in Svalbard (78º55' N, 11º55' E,
198 Fig. 1). Samples were collected between February 11 and 15 (*dark* campaign) and between April
199 9 and May 5 (*spring* campaign) during 2010. The sampling was undertaken at mid-day (11:00-
200 13:00) during the *dark* campaign, and every morning (09:00 – 10:00) during the *spring*
201 campaign. All snow samples were collected by inserting a pre-cleaned acrylic collars (height:
202 5cm, inner diameter: 10.4 cm, volume: 425 cm^{-3}) vertically into the snowpack, and using pre-
203 cleaned plastic shovels, clean overalls, face masks and powder-free gloves. Triplicate samples
204 were collected approximately 10 m apart, resulting in a total of 96 samples. To account for
205 variations in surface snow density throughout the campaign, several collars were filled next to

206 each other at each of the three triplicate sample locations, yielding a total sampled snow volume
207 between 1.3 L and 3.8 L. The snow was transferred directly into clean black plastic zipper
208 storage bags to prevent further photolysis, brought into the laboratory in Ny-Ålesund and melted
209 at room temperature. Each melted snow sample was vacuum filtered (pore size 0.45 μm,
210 according to Hodson et al., 2005), bottled in 50 ml-tubes, refrozen and shipped for analysis of
211 major ions and NO_3^- stable isotopes. To minimize contamination between samples, vacuum units
212 and sample tubes were rinsed three times with sample water or, in the case of low sample
213 volume, ultra-pure water (>18 MΩ). Field-blanks were collected along with the samples to check
214 for contamination. Blank bags were opened and closed during sampling (without any snow
215 addition), filled with 100 mL ultra-pure water, and then treated and analysed like the rest of the
216 samples. Furthermore, during the spring campaign, an extra 50 ml sterile sampling tube was
217 filled with the top 5 cm surface snow next to each sampling point for an opportunistic
218 complementary major ion analysis performed on-site.

219 2.2 Laboratory analysis

220 2.2.1 Major ions

221 The samples were analyzed for NO_3^-, chloride (Cl^-) and sodium (Na^+) by ion chromatography
222 at the Department of Geography, University of Sheffield, UK using two separate systems
223 (Dionex DX 90 ion chromatographs, 4400 integrators, AS40 autosamplers) with Dionex columns
224 AS14A and CS12A for anions and cations respectively. Standards (range 100 to 2000 μg L^{-1})
225 were prepared every day from 1000 mg L^{-1} Merck CertiPUR stock standards. The analytical
226 precision (1 standard deviation, 1σ) estimated from repeat analyses of multi element reference
227 standards (Merck CertiPUR) were 1.4 and 1.6 %, respectively, for the anions Cl^- and NO_3^-, and
228 0.06 % for the cation Na^+. Based on repeat analyses of separate filter aliquots, the analytical

229 precision including sample treatment was better than 5 % for each ion. Detection limits (D.L.)
230 defined as 3σ for the analytic blanks were 0.17, 0.21 and 0.34 μmol L^{-1} for Cl^-, NO_3^- and Na^+,
231 respectively.

232 The complementary spring-time 50 ml-snow samples and the diffusion line preparations
233 (described below in section 2.3.2) were analyzed for NO_3^-, Cl^-, Na^+, NO_2^- and bromide (Br^-) in
234 Ny-Ålesund by the Institute of Atmospheric Pollution Research – National Research Council of
235 Italy (IIA-CNR). Melted snow was analyzed without pre-treatment by ion chromatography
236 analytical technique (Dionex ICS 90 coupled with an AS50 auto-sampler and using Dionex
237 AS14 and CS12 columns). A multipoint calibration was performed using six standards in the
238 range 5 to 1000 μg L^{-1}, obtaining linear responses. Dilutions were carried out for more
239 concentrated samples. Calibration solutions were prepared every second week from 1000 mg L^{-1}
240 standard solutions (Merck). Control samples (1000 μg L^{-1} calibration solution) were analyzed
241 every seven samples in order to re-calibrate the ion chromatograph. The variation in the
242 concentration of these control samples ranged within 0.5 – 1 %. The analytical precision errors
243 from repeated analyses of a calibration solution (500 μg L^{-1}), were 1.13, 0.73, 0.35, 0.43 and
244 1.31 %, respectively, for Cl^-, NO_2^-, Br^-, NO_3^- and Na^+. Detection limits of 46. 5, 14.3, 4.9, 6.9
245 and 35.8 nmol L^{-1} were determined for Cl^-, NO_2^-, Br^-, NO_3^- and Na^+, respectively.

246 2.2.2 NO_3^- isotopic composition

247 The ^{15}N and ^{18}O isotopic composition of NO_3^- were analyzed at the School of Environmental
248 Sciences, University of East Anglia, Norwich, UK, using the bacterial denitrifier method
249 (Sigman et al., 2001; Coplen et al., 2004; Kaiser et al., 2007) where the *Pseudomonas*
250 *aureofaciens* strain was utilized. Values presented here are denoted as isotope deltas, $\delta(^{15}N)$ and

$\delta(^{18}O)$ (IUPAC nomenclature: $\delta(^{15}N, {}^{14}N, NO_3^-)$ and $\delta(^{18}O, {}^{16}O, NO_3^-)$, respectively), and expressed with respect to an international standard in ‰ (10^{-3}, per mil) (Eq. 1).

$$\delta_{\text{sample}} = \frac{R_{\text{sample}} - R_{\text{ref}}}{R_{\text{ref}}} \quad \text{Eq. 1}$$

Here R represents the $^{15}N/^{14}N$ or $^{18}O/^{16}O$ ratio in the sample ($_{\text{sample}}$) and reference ($_{\text{ref}}$) respecively, where atmospheric nitrogen (Air-N_2) was used as nitrogen reference and Vienna Standard Mean Ocean Water (VSMOW) was used as oxygen reference. Positive delta values indicate an enrichment of the heavier isotope (or a depletion of the lighter isotope) compared to the standard. To calibrate the isotope delta values, the international nitrate reference material IAEA-NO-3 was used, assuming it has $\delta(^{15}N)$ = 4.7 ‰ vs. Air-N_2 and $\delta(^{18}O)$ = 25.61 ‰ vs. VSMOW (Böhlke et al., 2003). The $\delta(^{15}N)$ values reported here have not been corrected for any non-mass dependent ^{17}O contribution to the m/z 45 ion current during mass-spectrometric analysis. However, $\delta(^{17}O)$ and $\delta(^{18}O)$ are usually well correlated and the true $\delta(^{15}N)$ was estimated to be 1-2 ‰ lower than the reported values. The bacterial denitrifier method requires a minimum of 20 nmol NO_3^- (optimum being 50 nmol) in at most 10 mL of solution. Consequently, only samples above this limit were analyzed (n = 87).

2.3 Air-snow fluxes

2.3.1 Surface snow net change

By following the concentration change in surface snow over time, it is possible to evaluate the overall net change due to surface snow processes occurring after wet deposition. This method has previously been used to evaluate NO_3^- dry deposition to snow (Cadle et al., 1985; Johansson and Granat, 1986; Cadle, 1991; Cress et al., 1995). The net change (F_{net}) can be calculated as (Björkman et al., 2013):

$$F_{\mathrm{net}} = -\frac{c_0 V_{\mathrm{t}} - c_{\mathrm{t}} V_{\mathrm{t}}}{At} \quad \text{Eq. 2}$$

where c is the molar NO_3^- concentration in snow, V the melted volume of the sample, A the surface area of the snow sample (in this study equal to the cross section area of the sampling collar), and where t is the exposure time between the initial sample (index: 0) and the final sample (index: t). In Björkman et al., (2013) the dry deposition was calculated as an atmospheric loss, giving negative numbers, whereas here the surface gain is of interest, hence a negative sign is used in Eq. 2 to account for this. Furthermore, Eq. 2 will be valid as a pure dry deposition estimate only if no other NO_3^- post-depositional processes take place and snow-water sublimation is negligible. In all other cases, Eq. 2 will describe the net effect of the various processes. In terms of the isotopic composition, Eq. 2 can be written as:

$$F_{\mathrm{net}}\,(1 + \delta_{\mathrm{net}}) = -k\,[c_0(1 + \delta_0) - c_t(1 + \delta_t)] \quad \text{Eq. 3}$$

where k is the deposition velocity given as: $k = V_{\mathrm{t}} / (At)$, δ_{net} is the isotopic composition of the net change, whereas δ_0 and δ_t are the initial and final isotopic composition of NO_3^-. Equation 3 can be expressed as:

$$0 = c_t(\delta_t - \delta_{\mathrm{net}}) - c_0(\delta_0 - \delta_{\mathrm{net}}) \quad \text{Eq. 4}$$

which then can be rearranged to give:

$$\delta_{\mathrm{net}} = \frac{c_t \delta_t - c_0 \delta_0}{c_t - c_0} \quad \text{Eq. 5}$$

Eq. 5 then gives the change in the isotopic signature (δ_{net}) and is equal to the isotopic composition of the dry deposited NO_3^- if other post-depositional processes are negligible.

2.3.2 NO_x, HNO_3^- and p-NO_3^- flux measurements

In addition to the snow sampling, atmospheric flux measurements of NO, NO_2, HNO_3 and p-NO_3^- to and from the snowpack were conducted by IIA-CNR outside Gruvebadet (200 m from

295 the snow sampling site) during the period April 9 to 27 in 2010. The NO and NO_2 concentrations
296 were measured on a 6 minute basis, using a modified commercial two-channel high-sensitivity
297 chemiluminescence detector (Sonoma Technologies, USA, Beine et al., 2002b; Amoroso et al.,
298 2010). The two channels sampled air from dual inlets at 0.3 m and 1.5 m above the surface snow,
299 respectively. Nitric oxide detection was based on the chemiluminescence signal produced by the
300 reaction between NO and O_3, which was photolytically generated in a 150 ml min^{-1} flow rate of
301 O_2 by a corona discharge O_3 generator. Nitrogen dioxide was detected as NO following
302 photolysis between 350 and 420 nm by light-emitting diodes. The instrument was calibrated
303 daily with 5.0 μmol mol^{-1} of gaseous NO (NIST traceable NO standard, Scott-Marrin, in N_2) at a
304 flow rate of 2.0 ml min^{-1} into the sampling flow (about 1200 ml min^{-1}), corresponding to a NO
305 addition of 8.3 nmol mol^{-1}. The NO detection limit was determined as 3σ of the observed scatter
306 in the instrument signal and corresponded to 2.5 pmol mol^{-1} for 1 h averages.

307 Measurements of HNO_3 and p-NO_3^- concentrations were made by two independent diffusion
308 lines (Beine et al., 2001; Perrino et al., 2001; Ianniello et al., 2002; Ianniello et al., 2007) with
309 inlets also at 0.3 and 1.5 m above the snow surface. The HNO_3 and p-NO_3^- concentration was
310 measured on a 12 h basis from April 10 to 16, while a time resolution of 24 h was used from
311 April 17 to 27. The diffusion lines used in this study included a denuder train consisting of two
312 sodium fluoride (1% NaF in 9:1 ethanol/water solution) coated denuders for HNO_3 sampling.
313 The atmospheric HNO_3 concentrations were calculated by subtracting the analyte mass
314 (expressed as NO_3^-) in the second NaF coated denuder from the analyte mass in the first NaF
315 coated denuder (Febo et al., 1989). The denuder train was followed by a cyclone (2.5 μm
316 aerodynamic diameter cut-off point) and a filter pack set in series, for the collection of
317 particulate matter in the coarse and fine fractions, respectively. The filter pack included a Teflon

318 filter (Whatman Teflon, 47 mm, 1 μm pore size), a nylon filter (Nylosorb Gelman, 47 mm, 1 μm
319 pore size), a Na_2CO_3-glycerol impregnated paper filter (Whatman 41) and a H_3PO_3 coated paper
320 filter. The last three filters were used to collect chemical species evaporated from the Teflon
321 filter (Ianniello et al., 2002; Ianniello et al., 2011; Spataro et al., 2013). The sampling flow rate
322 was 15 L min^{-1}, and typical sampling volumes of 11.9 m^3 and 23.5 m^3 were obtained for 12 h and
323 24 h sampling periods, respectively. After sampling, the denuders, cyclone and filters were
324 extracted and these samples were analyzed within 24 h by using the IIA-CNR Ion
325 Chromatography system described in section 2.2.1. Under these conditions, the collection
326 efficiency for both HNO_3 and p-NO_3^- was >99%. The D.L. of HNO_3 and p-NO_3^- (calculated as
327 3σ of field blanks) were 2.95 ng m^{-3} and 1.42 ng m^{-3}, respectively on a 24 h measurement period,
328 while the precision errors of these measurements were 2.54 % at 20 ng m^{-3} and 0.73 % at 79 ng
329 m^{-3}, respectively. Here we focus only on HNO_3 and p-NO_3^- data, although the diffusion line
330 sampling system did allow us to also collect other gaseous and particulate compounds, which
331 will be discussed elsewhere.

332 The fluxes of NO, NO_2, HNO_3 and p-NO_3^- (hereafter F_{NO}, F_{NO2}, F_{HNO3} and $F_{p\text{-}NO3}$,
333 respectively) were determined combining the two height gradient sampling with atmospheric
334 turbulence measurements. The difference between the measured concentrations at the two
335 sampling heights is in this work referred to a concentration difference (Δ = lower height – upper).
336 Hence, a positive difference implies emission of the measured species from the snow surface.

337 Using the measured concentration differences and the atmospheric eddy diffusivities (K) for
338 the same period, the atmospheric fluxes for NO, NO_2, HNO_3 and coarse and fine particulate NO_3^-
339 were derived (Flux = $\Delta \times K$) as detailed elsewhere (Sozzi et al., 1998; Ianniello et al., 2002;
340 Beine et al., 2003 and references therein). Diffusivities were obtained from atmospheric

341 turbulence measurements made at a frequency of 10 Hz by using an UVW tripropeller
342 anemometer (Metek, USA-T1), which was placed at 1.5 m above the snowpack, assuming
343 neutral boundary layer conditions.

344 For the purpose of this study these fluxes have been averaged to daily emissions, depositions
345 and net fluxes (from 09:00 onwards) for comparison with the surface snow data.

346 2.3.3 Dry deposition estimates

347 If the atmospheric concentration (c_{atm}) of HNO_3 and p-NO_3^- are measured, the expected dry
348 deposition flux ($F_{dry\text{-}dep}$) can be modeled as long as the deposition velocities (v_d) are known (e.g.
349 Seinfeld and Pandis, 2006):

350 $$F_{dry-dep} = v_d c_{atm} \quad \text{Eq. 6}$$

351 In a recent study covering the same *spring* campaign, the dry deposition of HNO_3 and p-
352 NO_3^- was both modelled and measured for Ny-Ålesund (Björkman et al., 2013). Median
353 deposition velocities were estimated to be 0.63 cm s^{-1} for HNO_3 and 0.0025 or 0.16 cm s^{-1} for p-
354 NO_3^-, particle size 0.7 and 7 μm in diameter, respectively (Björkman et al., 2013). The combined
355 gaseous and particulate dry deposition, F_{model}(LND) (referring to the modelled HNO_3 and p-NO_3^-
356 dry deposition rates obtained using a lognormal distribution (LND) for NO_3^- aerosols sizes in
357 Björkman et al., (2013)), will be used here for comparison with the surface snow and flux
358 measurements, and for further modelling purposes. Björkman et al., (2013) also measured the
359 actual NO_3^- dry deposition (F_{tray}) to snow using a "bucket" approach (e.g. Cress et al., 1995) and
360 found an average deposition of (0.04±0.02) mg m^{-2} d^{-1} (equal to (0.7±0.3) μmol m^{-2} d^{-1}) which
361 will also be used for further modelling purposes. An overview of NO_3^- dry deposition in the
362 Arctic, and a full description of these dry deposition estimates are given by Björkman et al.
363 (2013).

364 2.3.4 Additional observations

365 Meteorological data from Ny-Ålesund, in particular precipitation data, were provided by the
366 Norwegian Meteorological Institute (DNMI) and are available at http://*www.eklima.no*. The
367 atmospheric concentration of O_3 (c_{O3}) is continuously measured by the Norwegian Institute for
368 Air Research (NILU) at the nearby Zeppelin atmospheric research station (474 m a.s.l, Fig. 1),
369 available at *http://ebas.nilu.no*. During the spring campaign 2010, O_3 concentrations were also
370 recorded by IIA-CNR at Gruvebadet until April 27. NILU also provides an online base
371 atmospheric transport model, FLEXTRA (*http://www.nilu.no/projects/ccc/trajectories/*). Using
372 FLEXTRA air mass back-trajectories arriving to Ny-Ålesund were established for all sampling
373 days at 00:00 and 12:00, with trajectories spanning 7 days back in time.

374 Additionally, sonic anemometer (Gill R3) and fast hygrometer (Campbell Scientific KH2O
375 krypton) data from the Amundsen-Nobile Climate Change Tower (Fig. 1) were provided by The
376 Institute for Atmospheric Science and Climate - National Research Council of Italy (ISAC-CNR,
377 M. Mazzola and A. Viola, per. com.). The 10 minute average data sampled at 7.5 m above
378 ground were used to evaluate water vapour flux as an indication of sublimation rates.

379 2.4 Models

380 2.4.1 Photolytic model

381 NO_x production due to photolysis of NO_3^- has previously been modelled for Ny-Ålesund
382 snow, using the solar zenith angle (θ_{SZA}) and the surface snow NO_3^- concentrations, with results
383 comparable to NO_x emission measurements (France et al., 2010; France et al., 2011b). This
384 model assumes that the photolysis of NO_3^- only follows the reaction $NO_3^- + h\nu \rightarrow NO_2 + O^-$ and

385 is, according to the reactions in Fig. 2, a simplification of the DI dynamics, but has the potential
386 to provide useful insights into the NO_3^- loss through photolysis. For the purpose of this study, a
387 photolytic rate function considering only the surface snow layer during clear sky conditions
388 (France et al., 2010) will be used for comparison to the sampled top 5 cm of the snowpack.
389 However, a depth integrated model would be more appropriate if bulk snowpack samples were
390 under consideration (see France et al., 2010; France et al., 2011a; France et al., 2011b for further
391 details). Here only surface snow was sampled, in order to avoid a potential disturbance of the
392 post-depositional processes under investigation.

393 A polynomial function (Eq. 7) was fitted to the photolysis rates (J_{NO3-}, in s^{-1}) given in
394 France et al. (2010) as a function of θ_{SZA} (in º), with R^2= 0.9994 (Fig S1):

395 $$J_{NO_3^-} = 1.18e^{-14}\theta_{SZA}{}^4 - 1.09e^{-12}\theta_{SZA}{}^3 - 3.51e^{-11}\theta_{SZA}{}^2 - 8.80e^{-10}\theta_{SZA} + 3.86e^{-7} \quad \text{Eq. 7}$$

396 where θ_{SZA} was extracted for Ny-Ålesund (*http://www.esrl.noaa.gov/gmd/grad/neubrew/*) with 1
397 h resolution. Furthermore, to not induce any error from Eq. 7 when the sun is close to or below
398 the horizon, J_{NO3-} was set to zero for θ_{SZA} > 89.77º.

399 The upper limit for the surface snow NO_2 emission ($F_{J\,NO3-}$) can then be calculated as:

400 $$F_{J_{NO_3^-}} = J_{NO_3^-} c_0 z_{SWE} \quad \text{Eq. 8}$$

401 where c_0 is the concentration of NO_3^- (in mol m^{-3}) and z_{SWE} is the snow water equivalence of the
402 surface snow (in m). For lower NO_3^- concentrations, or unusually high NO_2 emissions, the
403 surface snow NO_3^- concentration might change over the course of the day. To minimize this
404 potential source of error, the time resolution of the photolysis calculations was set to 1 h in
405 accordance with the θ_{SZA} data. The $F_{J\,NO3-}$ emission given by Eq. 8 provides the flux in µmol m^{-2}
406 d^{-1} units.

2.4.2 Box models

A box model, describing the main sources and sinks of NO_3^- in the snow, was applied to predict changes in concentration (c_{NO3}), $\delta(^{15}N)$ and $\delta(^{18}O)$ of NO_3^-. In this box model all outgoing fluxes were assumed to be due to photolysis of NO_3^-, and all incoming fluxes were assumed to be due to NO_3^- dry deposition. Hence, this is a simplification of the actual processes, which might for example also include evaporation of HNO_3 (see Fig. 2). However, as an initial assumption (and further justified below) photochemistry was assumed to be the major loss process for this surface snow study.

In the model, the change in c_{NO3} over time when the sun is below the horizon was expressed as Eq. 9, while Eq. 10 gives the change when both dry deposition and photolysis are present:

$$\frac{dc}{dt} = \frac{v_d c_{atm} A}{V_t} \quad \text{Eq. 9}$$

$$\frac{dc}{dt} = \frac{v_d c_{atm} A}{V_t} - Jc \quad \text{Eq. 10}$$

Here $v_d c_{atm}$ equals the dry deposition rates according to Eq. 8, and was attributed to the F_{model}(LND) or F_{tray} in Björkman et al. (2013), while the product of photolytic rate (J) and snowpack concentration (c) constitutes the loss process. Note, in Eq. 10 and the following equations the photolytic rate of NO_3^- (J_{NO3-} in Eq. 7) has been substituted with J to keep the equations simple. Equations 9 and 10 can be integrated to give the new concentration (c_t):

$$c_t = \frac{v_d c_{atm} A t}{V_t} + c_0 \quad \text{Eq. 11}$$

$$c_t = \left(\frac{v_d c_{atm} A}{V_t J}\right) * (1 - e^{-Jt}) + c_0 e^{-Jt} \quad \text{Eq. 12}$$

where Eq. 11 and 12 represent periods when the sun is below or above the horizon, respectively. The isotopic composition of NO_3^- remaining in the snow (δ_t) can then be expressed as:

$$\delta_t = \left(\frac{c'_t}{c_t} - 1\right)/R_{\mathrm{ref}} \quad \text{Eq. 13}$$

Similarly to Eq. 11 and 12, c'_t are given by:

$$c'_t = \frac{v_{\mathrm{d}} c'_{\mathrm{atm}} A t}{V_t} + c'_0 \quad \text{Eq. 14}$$

$$c'_t = \left(\frac{v_{\mathrm{d}} c'_{\mathrm{atm}} A}{V_t J'}\right) * \left(1 - e^{-J' t}\right) + c'_0 e^{-J' t} \quad \text{Eq. 15}$$

where $c'_0 = c_0 R_{\mathrm{ref}}(1+\delta_0)$, $c'_{\mathrm{atm}} = c_{\mathrm{atm}} R_{\mathrm{ref}}(1+\delta_{\mathrm{atm}})$, $J' = J(1+\varepsilon)$, and where δ_0 and δ_{atm} are the initial and atmospheric N or O isotopic composition, respectively, while ε is the photolytic fractionation for $^{15}N/^{14}N$ ($^{15}\varepsilon$) and $^{18}O/^{16}O$ ($^{18}\varepsilon$). Primed quantities refer to the less abundant isotopic species (^{15}N or ^{18}O). The error due to the assumption that the concentration of the major isotope is equal to the total nitrate concentration, is negligible (<0.01 ‰).

In order to evaluate the daily $\delta(^{15}N)$, $\delta(^{18}O)$ and c_{NO3} changes from the NO_x, HNO_3^- and p-NO_3^- flux measurements (section 2.3.2), the daily averaged emissions (F_{emi}) and deposition (F_{dep}) were evaluated in a similar way:

$$c_t = \frac{F_{(\mathrm{dep})} A t}{V_t} - \frac{F_{(\mathrm{emi})} A t}{V_t} + c_0 \quad \text{Eq. 16}$$

$$c'_t = \frac{F'_{(\mathrm{dep})} A t}{V_t} - \frac{F'_{(\mathrm{emi})} A t}{V_t} + c'_0 \quad \text{Eq. 17}$$

where $F'_{(\mathrm{dep})} = F_{(\mathrm{dep})} R_{\mathrm{ref}}(1+\delta_{\mathrm{atm}})$, $F'_{(\mathrm{emi})} = F_{(\mathrm{emi})} R_{\mathrm{ref}}(1+\delta_{\mathrm{photo}})$, and δ_{photo} is the isotopic composition of the instantaneous photolytic product: $\delta_{\mathrm{photo}} = \delta_0(1+\varepsilon)+\varepsilon$.

Previous studies have suggested a range of $^{15}\varepsilon$, from –48 ‰ (Frey et al., 2009) to –12 ‰ (Blunier et al., 2005), and $^{18}\varepsilon$ from –34 ‰ (Frey et al., 2009) to between 2 and 7 ‰ (McCabe et al., 2005) for the photolytic fractionation in question. However, secondary reactions (e.g. $NO_2 + OH^- \rightarrow NO_3^-$) following photolysis will generate an exchange of O (see DI reactions in Fig. 2,

Jacobi and Hilker, 2007) suggesting that any measured estimation of $^{18}\varepsilon$ will represent the combined effect of both the photolytic fractionation and secondary reactions (McCabe et al., 2005; Erbland et al., 2013). For the purpose of this study, $^{15}\varepsilon$ and $^{18}\varepsilon$ were set to –48 and 2 ‰, respectively (McCabe et al., 2005; Frey et al., 2009). Furthermore, a sensitivity test covering a range from 0 to –70 ‰ for $^{15}\varepsilon$ and 10 to –50 ‰ for $^{18}\varepsilon$ was also performed to evaluate the actual influence of different photolytic fractionations on the results.

Furthermore, three δ_{atm} deposition scenarios for each isotope composition, $\delta(^{15}N)$ and $\delta(^{18}O)$, were evaluated with the aim of establishing the most likely input source, so called "end-member", signatures for any dry deposition. For $\delta_{atm}(^{15}N)$ these scenarios were set to resemble: I) the local biogeochemical signal (+5 ‰), II) the ambient atmospheric signal (–13 ‰) described for Ny-Ålesund by Amoroso et al. (2010), and III) the influence of Polar basin air (–20 ‰) suggested by Morin et al. (2009). For $\delta_{atm}(^{18}O)$ the scenarios were set to resemble: I) the low $\delta(^{18}O)$ signal found in HNO_3 at Summit, Greenland (+40 ‰) due to the interaction with OH during NO_x-cycling and removal (see Fig. 2, Jarvis et al., 2009), II) the mid-latitude HNO_3 signal (+75 ‰) found in air arriving at Svalbard (Morin et al., 2009), and III) the uniquely high $\delta(^{18}O)$ found for HNO_3 in the polar basin atmosphere during spring due to the influence of the BrO-pathway (up to +100 ‰, Morin et al., 2009).

3. Results

3.1 NO_3^- concentrations

The surface snow NO_3^- concentrations (c_{NO3}) during the *dark* (n = 14) and the *spring* (n = 79) campaign averaged (2.9±0.2) µmol L^{-1} and (1.7±0.1) µmol L^{-1}, respectively (where the uncertainty denotes the standard error, $\sigma_{\bar{x}}$), with a total concentration range from 0.6 to 6.3 µmol

473 L^{-1} (Fig. 3e). The variations among the three replicates, sampled approx. 10 m apart, were
474 moderate (average $\sigma_{\bar{x}} = 0.3$ μmol L^{-1}) with some exceptions (maximum $\sigma_{\bar{x}} = 1.4$ μmol L^{-1} on
475 April 9), as viewed by the occasionally increased $\sigma_{\bar{x}}$ in Fig. 3e. The c_{NO3} variation found is larger
476 than the errors expected from IC analysis itself and therefore shows that local variation and the
477 layering of the surface snow have a large influence. During both the *dark* and the *spring*
478 campaign, several precipitation events occurred (Fig. 3e) which introduced new snow layers with
479 event-specific NO_3^- concentration and isotopic signature. These events interrupted any trends
480 that post-depositional processes would have introduced to the surface snow chemistry, and the
481 spring data were therefore separated into three distinct, precipitation-free periods: April 12-21,
482 23-26 and April 27 - May 5 (Fig. 3). Periods 1 and 2 were characterized by multiple surface
483 snow layers, whereas period 3 followed a large (> 5 cm) precipitation event resulting in a
484 relatively uniform snow surface (Fig. 3a). Period 3 was therefore considered the most reliable
485 period for identification of c_{NO3} and isotope composition trends.

486 For the *spring* campaign, linear regression models fitted to all three periods showed
487 significant increases in the surface snow c_{NO3} (Fig. 3e and Table 1), indicative of net deposition
488 or snow-water sublimation (see section 3.4). No such changes were found during the short *dark*
489 sampling campaign due to interrupting precipitation events. In general, all three spring periods
490 indicated a day to day c_{NO3} variation. To avoid any bias caused by such variation the fitted linear
491 regression models were used to calculate initial (index: 0) and final (index: t) values of c_{NO3} (and
492 other relevant parameters) for each period and will be used for modelling purposes (Table 1 and
493 2).

494 3.2 NO_3^- isotopic composition

The $\delta(^{15}N)$ of NO_3^- ranged between –15.9 and –13.7 ‰ during the *dark* sampling (n = 12), and between –19.9 and 0.7 ‰ during the *spring* campaign (n = 71), averaging (–14.7±0.2) ‰ and (–8.7±0.5) ‰ respectively (Fig. 3d). The $\delta(^{18}O)$ ranged between 76.6 and 83.7 ‰ during the *dark* sampling, and 76.5 to 90.6 ‰ during the *spring* campaign, averaging (79.2±0.6) ‰ and (85.1±0.4) ‰ respectively (Fig. 3d). In summary, the *spring* snow has significantly elevated values of $\delta(^{15}N)$ and $\delta(^{18}O)$ compared to the *dark* sampling (p-value < 0.01), although both periods showed considerable variability.

Linear regression models revealed significant increases of $\delta(^{15}N)$ and $\delta(^{18}O)$ during period 3 (Table 1), and to a lesser extent (p-value = 0.08) for $\delta(^{18}O)$ during period 2 (Fig. 3d and Table 1). The remaining linear regression models fitted for $\delta(^{15}N)$ and $\delta(^{18}O)$ during period 1 and 2 were not significant (Fig. 3d and Table 1). In a similar manner to c_{NO3}, the initial and final $\delta(^{15}N)$ and $\delta(^{18}O)$ values were calculated for each period using the linear regression models (Table 1 and 2) to minimize the effects of daily variability upon further calculations.

3.3 Snow Br^- and atmospheric O_3 concentrations

In contrast to c_{NO3}, surface snow concentration of Br^- (c_{Br}) showed an overall linear decline, particularly during period 2 and 3 (Fig. 3b and Table 1). This decline was in clear contrast to the observed sea-salt deposition, as shown by the linear regression models fitted to the surface snow Na^+ and Cl^- concentrations (c_{Na} and c_{Cl}, respectively in Table 1). The most likely explanation for this c_{Br} depletion involves BrO chemistry (discussed in section 4.4), which is typically connected to changes in atmospheric O_3 concentration (c_{O3}). The ambient c_{O3} showed evidence for several ozone depletion events (ODEs) during the *spring* campaign. These ODEs mainly occurred during period 2 and 3, and were commonly associated with air mass back-trajectories arriving from the polar basin (Fig. 3b and c).

518 3.4 Sublimation rates

519 The measurement of water vapour fluxes during the campaign was challenging due to
520 riming or fog on the optical windows of the fast hygrometer, meaning that calibration was not
521 always possible, which reduced the number of valid measurements. The removal of outliers from
522 the sonic anemometer data further reduced the data to a final count of 282 measurements
523 throughout the precipitation free sub-periods. Nevertheless, the data confirm a low sublimation
524 rate: the water vapor fluxes indicated an average sublimation rate of (–0.042±0.002) mm d^{-1} (n =
525 282), where the total water vapor flux spanned between –0.007 and 0.008 mm h^{-1} (negative flux
526 indicates surface loss). This sublimation rate has a very small impact on surface snow NO_3^-
527 concentration as discussed below.

528 3.5 Air-snow fluxes

529 3.5.1 Surface snow net change

530 The increasing trends in surface snow c_{NO3} indicate a net deposition of NO_3^- since snow-
531 water sublimation was found to be low. Hence, this indicated that dry deposition rates overcome
532 photolytic and evaporative losses. Using the calculated initial and final values of c_{NO3} and V for
533 each period (Table 2), all three period were confirmed to have a significant increase due to net
534 deposition according to Eq. 2 (Table 3). Similarly the isotopic composition for the net change
535 was calculated according to Eq. 5 (Table 3).

536 3.5.2 NO_x, HNO_3^- and p-NO_3^- flux measurements

537 The mean NO_2 concentrations (C_{NO2}) during the campaign were 28.6 (σ = 19.3) pmol
538 mol^{-1} and 28.7 (σ = 20.3) pmol mol^{-1} at the upper and lower inlet, respectively (Fig. 4a).
539 Similarly, the mean NO concentrations (C_{NO}) were 15.2 (σ = 12.5) and 16.6 (σ = 17.5) at the
540 upper and lower inlet respectively (Fig. 4b). The C_{NO} and C_{NO2} concentrations showed

541 statistically significant diurnal cycles on some days (9-11 April, 15-16 April, 22-27 April) with
542 amplitudes of 1-36 pmol mol^{-1} and 3-49 pmol mol^{-1} for C_{NO} and C_{NO2}, respectively (Fig. 4a, b).
543 The diurnal cycles appeared more or less symmetric with UV radiation, with maximum C_{NO} and
544 C_{NO2} observed between 11:00 and 13:00, reaching minima values during night-time. During
545 periods without diurnal cycles the maximum NO and NO_2 concentrations were reached between
546 18:00 and 21:00, with minimum values measured between 06:00 and 12:00 and, hence, delayed
547 the diurnal irradiance pattern. The turbulence measurements resulted in median eddy diffusivity
548 (K) of 0.2 mol m^{-2} s^{-1} (with the first and third quartile at 0.14 and 0.22 mol m^{-2} s^{-1}, respectively),
549 and the NO_x, HNO_3 and p-NO_3^- fluxes were calculated as K multiplied by the difference between
550 the two inlets (as detailed in Beine et al., 2003). The 6 min NO_x fluxes data (Fig. 4c) showed a
551 median NO emission of – 0.73 pmol m^{-2} s^{-1} (with the first and third quartile at – 0.31 and – 1.53
552 pmol m^{-2} s^{-1}, respectively) with a median NO_2 emission of – 0.79 pmol m^{-2} s^{-1} (with the first and
553 third quartile at – 0.35 and – 1.62 pmol m^{-2} s^{-1}, respectively). The corresponding median NO
554 deposition rates (Fig. 4c) were 0.61 pmol m^{-2} s^{-1} (with the first and third quartile at 0.27 and 1.18
555 pmol m^{-2} s^{-1}, respectively) while the median NO_2 deposition was 0.83 pmol m^{-2} s^{-1} (with the first
556 and third quartile at 0.38 and 1.54 pmol m^{-2} s^{-1}, respectively). The combined daily fluxes of NO_x
557 (F_{NOx}), used for comparison to the surface snow concentrations (Fig. 5b), showed an daily
558 averaged F_{NOx} emissions range from –0.2 to –1.8 μmol m^{-2} d^{-1}, and the daily average F_{NOx}
559 depositions ranged from 0.2 to 1.7 μmol m^{-2} d^{-1} (Fig. 5b). The resulting daily net fluxes (ΣF_{NOx})
560 ranged from –0.1 to 0.2 μmol m^{-2} d^{-1} (Fig. 5b).

561 The mean concentrations of HNO_3, fine and coarse particulate NO_3^- were 6.06 ± 5.32,
562 14.33 ± 13.68 and 15.14 ± 9.53 ppt, respectively. The HNO_3 and the combined fine and coarse
563 particulate NO_3^- fluxes (F_{HNO3} and $F_{p\text{-}NO3}$, Fig. 5c) mostly indicated a deposition, with the mean

values of 1.59 ± 1.32 pmol m^{-2} s^{-1} and 4.84 ± 3.52 pmol m^{-2} s^{-1}, respectively. The resulting daily net flux of the total HNO_3 and p-NO_3^- (ΣF_{NO3}) showed variable rates, from – 0.6 to 3.2 μmol m^{-2} d^{-1} (Fig. 5c), where the flux of p-NO_3^- ($F_{p\text{-}NO3}$) exceeded that of HNO_3 (F_{HNO3}) and thus dominated ΣF_{NO3}, with particularly high rates during the precipitation event between period 2 and 3 (Fig. 5c). The data also shows that fine particles (<2.5 μm diameter) were responsible for much of the p-NO_3^- flux during high flux events. The sampling interval (12 or 24 h) for F_{HNO3} and $F_{p\text{-}NO3}$ did not allow a separation of daily emission and deposition estimates, as was achieved using the 6 minute F_{NOx} data.

3.6 Box models

The photolytic rate function ($J_{NO3\text{-}}$) showed clear diurnal variation superimposed upon a uniformly increasing trend as a consequence of the steadily rising sun (midnight sun commenced on April 18). The integrated daily surface snow flux ($F_{JNO3\text{-}}$), estimated from $J_{NO3\text{-}}$ and c_{NO3}, showed emission rates of the same order of magnitude as the measured ΣF_{NOx}. However, $F_{J\,NO3\text{-}}$ was considerably lower than the measured NO_x emission (F_{NOx}). This mismatch is likely due to the estimation of NO_3^- photolysis from surface snow only being compared to measured emissions above the full snowpack.

The measured range of the combined HNO_3 and p-NO_3^- fluxes (ΣF_{NO3}) was of the same order of magnitude as the modelled HNO_3 + p-NO_3^- dry deposition (F_{model}(LND)) during this *spring* campaign (Björkman et al., 2013), although the measured average NO_3^- dry deposition (F_{tray}) showed higher spring averages than both F_{model}(LND) and the ΣF_{NO3} (Fig. 5c). However, the substantial atmospheric fluxes of HNO_3 and p-NO_3^- (F_{HNO3} and $F_{p\text{-}NO3}$) observed in connection with the precipitation event between period 2 and 3 was not captured by the dry deposition estimates in Björkman et al. (2013) (Fig. 5c).

587 4. Discussion

588 Here we present a discussion of the trends and influences on NO_3^- concentrations and
589 isotopic composition found for Ny-Ålesund surface snow. We argue that the main process during
590 precipitation free periods is the addition of NO_3^- through dry deposition, which dominates over
591 NO_3^- post-depositional losses via photolysis and evaporation. However, this dry deposition can
592 be influenced both by atmospheric sources, as well as NO_x, HNO_3^- and HONO emitted from
593 deeper within the snowpack, processes which therefore require consideration. An active
594 involvement of halogen chemistry was also inferred from the surface snow measurements, and so
595 we discuss the role of surface snow as a contributor in the production of boundary layer BrO.

596 4.1 Dry deposition vs. post-depositional loss

597 A striking feature during the *spring* sampling is the significant increase of c_{NO3} for all three
598 sub-periods, in-between precipitation events (Table 1 and Fig. 3e), where a positive net change
599 (F_{net}) was confirmed for all periods using Eq. 2 (Table 3). Hence, Eq. 2 gives the overall net
600 increase or decrease of c_{NO3}, where the most likely surplus would be due to an NO_3^- addition by
601 dry deposition as long as snow sublimation is low. The measured sublimation rates during the
602 three periods were low and could only have changed the daily c_{NO3} by a modest quantity
603 (average 0.31±0.03 %, range 0.2 to 0.8 %), which is well below the day to day c_{NO3} variations
604 (average 11.1±1.6 %, for the same periods). Similarly, the model photolysis rate ($J_{NO3\text{-}}$) could
605 only have changed the daily c_{NO3} by a 0.2 to 0.4 % reduction, indicating a very minor influence
606 of photolysis on these daily variations. Of course, HNO_3 evaporation and HONO emissions
607 could further influence the daily variations. However, both these processes require a surplus of
608 H^+, whereas Ny-Ålesund snow is typically alkaline (Beine et al., 2003; Amorosso et al., 2006)
609 with a high sea-salt content given the close proximity to the fjord. Furthermore, the NO_2^- levels

610 where below the detection limit of the IC measurements (data not shown) further indicating low
611 HONO production. The limited occurrence of sublimation, modelled J_{NO3-} and positive F_{net}
612 collectively therefore indicate that the addition of NO_3^- through dry deposition outweighed any
613 changes induced by photolytic and/or evaporative loss processes. The estimated F_{net} for the three
614 periods, with a daily-weighted average of 0.9±0.4 μmol m^{-2} d^{-1} (Table 3), is also consistent with
615 the measured dry deposition rate (F_{tray}, 0.7±0.3 μmol m^{-2} d^{-1}) estimated for the same time period
616 by Björkman et al. (2013). However, these are slightly higher than the average modelled dry
617 deposition (F_{model}(LND), 0.3±0.1 μmol m^{-2} d^{-1}) for this period (Björkman et al., 2013), and also
618 slightly higher than the value Beine et al. (2003) found for Ny-Ålesund (~0.2 μmol m^{-2} d^{-1})
619 during an previous spring, using a diffusion line sampling technique.

620 The $\delta(^{15}N)$ and $\delta(^{18}O)$ composition of the net change (δ_{net}), as calculated by Eq. 5, differed
621 between the three sub-periods (Table 3). Regarding the F_{net}, no major influence of loss processes
622 was found for periods 1 and 2, since any fractionation during post-depositional loss would have
623 led to an $\delta_{net}(^{15}N)$ increase in NO_3^-. In contrast, period 1 and 2 showed negative $\delta_{net}(^{15}N)$ values
624 of –8.2±13.6 and –12.2±18.8 ‰, respectively, even though the validity of these estimates are
625 reduced by the non-significant regressions used for calculation. One might argue that the
626 significant positive $\delta_{net}(^{15}N)$ value of (7.0±0.7) ‰ calculated for the NO_3^- in period 3 could be
627 indicative of post-depositional loss. This would, however, contradict the significant c_{NO3} increase
628 and positive F_{net} observed for this period (Table 3), therefore alternative explanations need to be
629 considered, as attempted through box modelling below. The NO_3^- $\delta_{net}(^{18}O)$ found for period 1,
630 even though the linear regression was non-significant, was lower than the isotope delta of the
631 snow (Table 3), whereas for periods 2 and 3 the $\delta_{net}(^{18}O)$ approached the upper limit found for
632 atmospheric HNO_3 in this region (100 ‰, Morin et al., 2009). The isotopic signature of snow

633 NO_3^- is, however, influenced by several co-occurring processes as discussed in the introduction
634 and viewed in Fig. 2 and will be further investigated in section 4.3.

635 4.2 NO_x, HNO_3^- and p-NO_3^- flux measurements

636 The flux measurements revealed both emissions and deposition fluxes of all the investigated
637 compounds (NO, NO_2, HNO_3^- and p-NO_3^-, Fig. 4 and 5) and where the mean NO and NO_2
638 concentrations were in agreement with other measurements in the coastal Arctic boundary layer
639 during the same time of year (Allegrini et al., 1999; Beine et al., 2001; 2002b; Amoroso et al.,
640 2010; Sander and Bottenheim, 2012). Although the calculated daily NO and NO_2 fluxes (Fig. 5)
641 are in the lower region of what has earlier been reported for Ny-Ålesund by Amoroso et al.
642 (2010), the occasional diurnal cycling of NO and NO_2 observed confirms previous studies
643 carried out at Ny-Ålesund (Beine et al., 1996 and 1997). Also the daily average HNO_3 flux
644 measured in 2010 are within the variability of earlier estimates for Ny-Ålesund (Beine et al.,
645 2003; Amoroso et al., 2010), but substantially lower than the episode with exceptionally high
646 deposition fluxes (up to 1.5 μmol m^{-2} h^{-1}) reported by Amoroso et al. (2010).

647 Due to coastal location of Ny-Ålesund, the chemical composition of snow was dominated by
648 a marine influence. As a result of sea salt inputs, and to a lesser extension of dust, the ionic
649 balance of snow revealed an alkaline character for 44% of the daily snow samples (with pH
650 values between 7.80 and 8.70) which, according to Beine et al. (2003 and 2008), could lead to a
651 reduced NO_x emission and even to an increased deposition. In addition, it is worth noting that
652 33% and 41% of all available 6-min NO and NO_2 fluxes (about 5000 values), respectively, were
653 positive values, indicating that a NO_x deposition to the snow surface occurred, as observed in
654 earlier polar studies (e.g: Beine et al., 2002, Amoroso et al., 2010). It has previously been shown
655 that the intricate system of NO_3^- photolysis and NO_x emission is followed by a subsequent HNO_3

deposition, producing a diurnal pattern at Summit, Greenland, with day-time emission and night time deposition (Hastings et al., 2004). A similar feature can be observed in our 2010 flux data, were the NO and NO_2 emission during periods of high irradiance can be on the same order of magnitude as the total HNO_3 and p-NO_3^- deposition. Indicating that, for this almost alkaline snow environment, the NO_x emissions were reduced or close to zero. Thus, the measured fluxes of NO_x, HNO_3 and p-NO_3^- are neither sufficient to explain the observed c_{NO3} increase. In the following section we will further focus on separating and explaining the processes influencing the surface snow, using the box model to find the most likely sources of the observed NO_3^- deposition and its isotopic signature.

4.3 Reproducing observed trends

In the box model used here, describing the main source and sink of NO_3^- in the snow (section 2.4.2), all outgoing fluxes are assumed to be due to photolysis and all incoming fluxes due to HNO_3 dry deposition. As a consequence of the day-to-day variability of isotope deltas and c_{NO3}, our comparison between model and measured data focuses on the regression analysis for the three precipitation-free spring periods, bearing in mind the lower p-values for the trends in $\delta(^{15}N)$ and $\delta(^{18}O)$ of snow NO_3^- during period 1 and 2 (Table 1 and Fig. 3).

4.3.1 Box model using F_{NOx} and F_{NO3}

The box model (Eq. 16) shows that the measured net fluxes of NO_x (ΣF_{NOx}, Fig 5b) and HNO_3 + p-NO_3^- (ΣF_{NO3}, Fig 5c) were insufficient to alter the surface snow c_{NO3} significantly during periods 1 and 2 (Fig. 6c, noting the atmospheric flux measurements were terminated on April 27, just prior to period 3). The small change in c_{NO3} such daily net fluxes would induce was below the detection limit of the snow sampling procedure used here. A similar conclusion was

678 reached by Beine et al., (2003) when they compared atmospheric dry deposition estimates with
679 the surface snow NO_3^- concentrations.

680 In spite of the limited ability of the atmospheric flux driven model to reproduce the
681 surface snow c_{NO3} trends, the modelled influence on $\delta(^{18}O)$ and $\delta(^{15}N)$ was more pronounced
682 (using Eq. 17, Fig. 6). This is especially the case during the first day of period 1, when p-NO_3^-
683 emission (Fig. 5c) resulted in an increased modelled $\delta(^{18}O)$, and where the $\delta_{atm}(^{18}O)$ scenarios
684 +40 and +100 ‰ followed the very lower and upper limit of the data variability for the rest of
685 period 1 (Fig. 6a). Although particle emission from snow might be limited (Cadle, 1991), some
686 re-suspension of particles by wind is possible (Barrie et al., 1998). During period 2 neither of the
687 $\delta_{atm}(^{18}O)$ scenarios followed the observed $\delta(^{18}O)$ pattern. For periods 1 and 2, the modelled $d^{15}N$
688 was not as sensitive to the choice of $\delta_{atm}(^{15}N)$ scenarios (+5, –13 and –20 ‰), as for $\delta(^{18}O)$. In
689 fact, model results for all three $\delta_{atm}(^{15}N)$ scenarios were well within the data variability and did
690 not deviate much from each other (Fig. 6b). Overall, none of the δ_{atm} scenarios and emission
691 fractionations, including the sensitivity test for different fractionations ($^{15}\varepsilon$ and $^{18}\varepsilon$, section 2.4.2),
692 reproduced the observed trends in a satisfactory way. This is probably due to the many layers
693 found in the sampled surface snow during period 1 and 2, that can yield large daily variations in
694 $\delta(^{15}N)$ and $\delta(^{18}O)$. It is especially troublesome that the observed c_{NO3} trends (Table 1) and
695 calculated dry deposition rates (Table 3) cannot be explained by the atmospheric flux in the box
696 model. A possible explanation could be a re-deposition of NO_x, HNO_3^- and HONO emitted from
697 deeper within the snowpack, or the soil below, to the surface snow layer. Such a sub-surface
698 source would then not necessarily need to involve an emission to the atmospheric boundary
699 layer, thus could impact the surface snow measurements of NO_3^- deposition but not the
700 atmospheric flux measurements as a result.

4.3.2 Box model using J_{NO3-} and F_{model}(LND) or F_{tray}

As a second attempt to reproduce the observed surface snow trends (Eq. 11 and 12) and to also address the observations of period 3, which can be considered most reliable as the surface snow was one homogeneous layer, the modelled photolysis (J_{NO3-}) was used in conjunction with F_{model}(LND), Fig. S2. This box modelling attempt, and a third approach, using J_{NO3-} in conjunction with F_{tray}, Fig. 7, captured the c_{NO3} trends far better than the atmospheric flux measurements. This was particularly the case with the third attempt, which reproduced the observed c_{NO3} increase during period 3 in a sufficient manner (Fig. 7), attributing the addition through dry deposition to have a prevailing role over photolytic and, probably, evaporative loss.

For the isotopic composition the models (Eq. 14 and 15) seems to have had a clear negative influence upon the surface $\delta(^{15}N)$ signature during periods 1 and 2 (Fig. S2 and 7), with a $\delta_{atm}(^{15}N)$ close to the ambient atmospheric (–13 ‰, Amoroso et al., 2010) and the Polar Basin signals (–20 ‰ , Morin et al., 2009). This also corresponds well to the main back-trajectories observed during these periods (Fig. 3c). In contrast, period 3 indicated the influence of a positive end-member (+7.0 ± 0.7 ‰, Table 3) that cannot be explained by a photolytic and/or evaporative NO_3^- loss, hence indicates dry deposition seems to have occurred. This positive $\delta(^{15}N)$ signature is more in line with the +5 ‰ previously described for snowpack biogeochemical processes in this region (Amoroso et al., 2010), indicating a re-deposition of NO_x, HNO_3^- and HONO emitted deeper within (or below) the snowpack. However, anthropogenic NO_x emissions are also in general slightly positive (e.g. Hastings, 2010), with the exception of agricultural soils (Felix and Elliott, 2013). For example, Morin et al., (2009) found an atmospheric nitrate signal of +5.9 ‰ from European air in the English Channel, a value also consistent with mid-latitude spring values for the U.S. (Elliott et al., 2009). For period 3, the air mass back-trajectories are more stagnant

around Svalbard, with a south-easterly influence at the end of this period. This indicates that the high end-member found for period 3 could also be influenced by local or European emission sources, and is not necessarily solely a biogeochemical signal.

For period 1, the $\delta(^{18}O)$ end-member is close to the mid-latitude scenario (+75 ‰, Fig. S2 and 7), which is also the post-1950 background value for this region as indicated by Svalbard ice-core averages (+75.1 ± 4.1 ‰, Vega, 2014), in spite of a northerly airflow which was assumed to bring a $\delta(^{18}O)$ signal around +100 ‰. The $\delta(^{18}O)$ end-member for period 2 and 3 is on the other hand more in line with air masses from the Polar Basin (Morin et al., 2009), for which the uniquely high $\delta(^{18}O)$ has been found to result from an active atmospheric BrO interaction (Fig. 2, Morin et al., 2007a; Morin et al., 2007b). This is especially surprising for period 3, where the back-trajectories are stagnant or south-easterly oriented, with only a minor influence of Polar air (Fig. 3c). Under these circumstances a mid-latitude $\delta(^{18}O)$ scenario would be expected for period 3, rather than the +100 ‰ evidenced here. The reason for this deviation is probably due to a local snow-determined BrO-NO_x interaction, the first such observation of its kind in this region, and will be further discussed in section 4.

The sensitivity test performed (shaded ranges in fig 6, 7 and S2) indicates that the actual photolytic fractionation used in the box modelling has little influence on the outcome, probably due to the prevailing dry deposition regime in our surface snow.

In summary; Period 1 shows evidence of a polar basin/ ambient atmospheric influence on $\delta(^{15}N)$ and a $\delta(^{18}O)$ signature that resembles mid-latitudinal air. Period 2 shows a polar basin influence upon both the $\delta(^{15}N)$ and the $\delta(^{18}O)$ signatures; whilst period 3 has a $\delta(^{15}N)$ similar to that which is expected from either biogeochemical cycling of NH_4^+ in the snowpack, or local/European emissions, along with the BrO influenced $\delta(^{18}O)$ signature.

747 4.4 O_3 and BrO interaction

748 During the *spring* campaign several O_3 depletion events (ODE) occurred; on April 13, 21
749 – 22, 26 – 27 and April 30 – May 1 (Fig. 3b). Such events are known in the Arctic as a result of
750 active halogen chemistry where Br_2, BrCl or Cl_2 (ultimately of oceanic origin, whose release is
751 believed to involve snow and first-year sea-ice) are released in to the boundary layer. Their rapid
752 photolysis by solar radiation forms Br or Cl radicals, which then initiates a chain reaction
753 depleting O_3 (Fig. 2, e.g. Foster et al., 2001; Simpson et al., 2007; Abbatt et al., 2012). For Ny-
754 Ålesund, studies typically observe such events as a consequence of the advection of air masses
755 already depleted in O_3, originating from the polar basin (e.g. Barrie and Platt, 1997), where low
756 levels of boundary layer O_3 are typical during spring (Hopper et al., 1994; Hopper et al., 1998;
757 Jacobi et al., 2010). This is consistent with the ODEs observed during the spring 2010, where
758 more northerly air flows occur prior to the ozone depletion episodes (Fig. 3) and where satellite
759 data (Begoin et al., 2010) reveals increased BrO column abundances concurrent with the ODE's
760 (Fig. S3). Alongside its impact on boundary layer O_3, BrO can also influence NO_x-cycling and
761 its transformation to HNO_3, via the formation and hydrolysis of $BrONO_2$. This generates a
762 uniquely high $\delta(^{18}O)$ (Fig. 2, e.g. Evans et al., 2003; Morin et al., 2007b).

763 For period 2 a northerly airflow was observed which can explain both the low $\delta(^{15}N)$
764 (photolytic produced NO_x from polar basin snowpacks) and the high $\delta(^{18}O)$ (BrO-pathway) end-
765 member (Morin et al., 2009). However, for period 3, when the airflow is stagnant or south-
766 westerly, with only a minor influence of polar basin air, the high $\delta(^{18}O)$ end-member would need
767 to have another explanation. Interestingly the Br^- concentrations (c_{Br}) in the surface snow are
768 high during period 1, decrease during period 2, then remain low and slightly decrease further
769 during period 3 (Fig. 3b and Table 1). There is also a significant ($p < 0.05$) negative correlation

between the daily averages of c_{Br} and c_{NO3} (R = –0.84) during period 3, as well as between c_{Br} and $\delta(^{15}N)$ and $\delta(^{18}O)$ (R = –0.91 and –0.83, respectively). According to the BrO-pathway in Fig. 2, formation of $BrONO_2$ from BrO + NO_2 can be followed by a photolytic dissociation, or – particularly under conditions of high surface area – be followed by hydrolysis whereby $BrONO_2$ disintegrates into HNO_3 and HOBr on ice crystals (Evans et al., 2003; Morin et al., 2007b). This latter case thereby converts NO_x into HNO_3. Assuming that this reaction occurs within the snow or just above, the newly formed HOBr would further react with Br^- ions in the DI with a release of gaseous Br_2 as a result (e.g. Simpson et al., 2007; Abbatt et al., 2012). In the presence of a NO_x, HNO_3 or HONO supply from deeper within the snowpack (i.e. photolysis, evaporation or biologic emissions from the snow or soil), this BrO-NO_x chemistry would rapidly re-deposit the NO_x as HNO_3 in the surface snow. This would then minimize any snowpack emissions and, in the case of negligible local soil emissions, keep the total snow NO_3^- budget un-altered. This coupled BrO-NO_x chemistry can explain both the decrease in Br^- concentration in the surface snow as well as the increasing $\delta(^{18}O)$ and c_{NO3} values observed in the surface snow during period 2 and 3. This is the first time such coupling has been observed in Svalbard, although increasing BrO levels have earlier been reported above Ny-Ålesund snow following an ODE (Avallone et al., 2003). To start the BrO production and following chain reactions, an initial pulse (or "seed") of reactive halogens is needed (Simpson et al., 2007). It is however, unlikely that the BrO cycling seen in our c_{Br} and $\delta(^{18}O)$ data, and in the BrO record from Avallone et al., (2003) are initiated locally. They are likely rather results of polar basin air advection providing "seed" halogens during the observed ODEs, which then initiate the local BrO production. This hypothesis is further strengthened by the column content of BrO (Fig. S3) where the atmosphere above western Svalbard, and eastern parts of the Fram Strait, shows prevailing low BrO levels,

793 which only increases in conjunction with ODE's when surges of BrO moves into the Ny-Ålesund
794 area. Nevertheless, during period 3, our surface snow bromide, nitrate, and $\delta(^{18}O)$ observations
795 provide evidence for continued local (snowpack) BrO-NO_x cycling, even whilst BrO column
796 abundances decline and ambient air ozone recovers.

797 5. Conclusion

798 Detailed sampling of the photo-active surface zone of the Ny-Ålesund snowpack during
799 winter and spring-time demonstrates that NO_3^- dry deposition is the predominant process
800 determining NO_3^- concentrations during precipitation free periods and prevails over any NO_3^-
801 post-depositional loss via photolysis and HNO_3 evaporation within this layer. The measured dry
802 deposition in uniform surface snow (0.6±0.2 μmol m^{-2} d^{-1}) is in line with previously reported
803 values for Ny-Ålesund (Björkman et al., 2013). However, it indicates greater net deposition than
804 that derived from cumulative NO_x, HNO_3^- and p-NO_3^- fluxes, measured 200 m from the sampling
805 site. Given its permeable nature, we emphasize that the snowpack should be considered as an
806 integral part of the atmospheric boundary layer, allowing relevant reactions (Fig. 2) to occur
807 within interstitial air pockets within the snow. Thus, our observed dry deposition of NO_3^- could
808 originate from both the overlying atmosphere and from re-deposition of NO_3^- released from
809 deeper within the snowpack.

810 Magnitudes and trends in surface snow $\delta(^{15}N)$ and $\delta(^{18}O)$ were compared to back-trajectory
811 analysis and local ODEs indicative of BrO chemistry. Trajectories originating from the polar
812 basin were found to bring ^{15}N-depleted air masses to Svalbard, confirming findings from an
813 earlier atmospheric study of NO_3^- in Ny-Ålesund aerosol (Morin et al., 2009), and demonstrating
814 that such NO_3^- is deposited to the snowpack. Stagnant air and air masses originating from mid-
815 latitude regions were related to ^{15}N-enriched dry NO_3^- deposition with an end-member of

816 (+7.0±0.7) ‰. Such positive $\delta(^{15}N)$ values have previously been found in European and U.S. air
817 (Elliott et al., 2009; Morin et al., 2009), probably as a result of anthropogenic emissions (e.g.
818 Kendall et al., 2007), but can also result from in-situ biogeochemical cycling of clay-bound NH_4^+
819 (Amoroso et al., 2010).

820 The average $\delta(^{18}O)$ values were lower during the winter-time compared to spring-time, when
821 NO_3^- deposition from polar basin air masses only exhibited positive $\delta(^{18}O)$ trends in conjunction
822 with low O_3 levels. These conditions indicate active halogen cycling and demonstrate the
823 importance of NO_x to NO_3^- formation via coupled BrO-NO_x chemistry (as identified in Ny-
824 Ålesund aerosol: Morin et al., 2009) for snow NO_3^- deposition. Furthermore, we identify
825 evidence for such BrO chemistry occurring within the snowpack (interstitial air pockets) itself,
826 and demonstrate its active involvement in the NO_3^- post-depositional cycling, as evidenced by
827 steadily decreasing snow Br^- content and increasing $\delta(^{18}O)$ and NO_3^- concentration in surface
828 snow samples. These are the first observations of such snowpack BrO-NO_x coupling in this part
829 of the Arctic. However, as indicated both by this and a previous study (Avallone et al., 2003),
830 local BrO production is concomitant with the arrival of BrO active O_3-depleted air, which
831 contributes the necessary "seed" halogens to get the local production initiated (Simpson et al.,
832 2007). This production might explain the uniquely high $\delta(^{18}O)$ end-member (+105.9±72.3 ‰)
833 found even during stagnant and south-easterly air influences, regions usually associated with
834 higher O_3 levels.

835 In summary, our study demonstrates how careful sampling of surface snow can provide
836 useful insights regarding atmospheric and snow processes controlling the fate of reactive
837 nitrogen in the Arctic including coupling of BrO-NO_x chemistry. In particular, our results

838 elucidate the relative importance of these processes for a snowpack located in a coastal region at
839 low altitude (Ny-Ålesund), in contrast to studies elsewhere (e.g. Greenland).

840 ## 6. Acknowledgements

841 This work was part of the international project *Sources, sinks and impacts of atmospheric*
842 *nitrogen deposition in the Arctic* (NSINK), and received financial support from the EU Marie
843 Curie Initial Stage Training Network Award (NSINK, FP7 215503). Fieldwork was supported by
844 Arctic Field Grant, Svalbard Science Forum. This work is also a contribution to *Cryosphere-*
845 *Atmosphere interaction in a changing arctic climate (CRAICC)* a Top-Level Research Initiative
846 (TRI). TJR acknowledges LABEX VOLTAIRE (VOLatils- Terre Atmosphère Interactions -
847 Ressources et Environnement) ANR-10-LABX-100-01 (2011-20). Logistic support was
848 provided by the staff at the Sverdrup Station, Norwegian Polar Institute. NILU is acknowledged
849 for providing the FLEXTRA trajectories and Zeppelin O_3 data, wears DNMI for providing
850 meteorological data. The authors are grateful for the support from Mauro Mazzola and Angelo
851 Viola (ISCA-CNR) for providing water vapour flux data and from Andreas Richter (University
852 of Bremen) contributing with the supplementary BrO-maps. This manuscript has also been
853 improved by comments from three anonymous reviewers.

854 ## 7. References

855 Abbatt, J. P. D., 1997: Interaction of HNO_3 with water-ice surfaces at temperatures of the free
856 troposphere. *Geophysical Research Letters,* 24: 1479-1482.
857 Abbatt, J. P. D., Thomas, J. L., Abrahamsson, K., Boxe, C., Granfors, A., Jones, A. E., King, M. D., Saiz-
858 Lopez, A., Shepson, P. B., Sodeau, J., Toohey, D. W., Toubin, C., von Glasow, R., Wren, S. N.,
859 and Yang, X., 2012: Halogen activation via interactions with environmental ice and snow in the
860 polar lower troposphere and other regions. *Atmospheric Chemistry and Physics*, 12: 6237-6271.
861 Albert, M. R. and Hardy, J. P., 1995: Ventilation experiments in a seasonal snow cover. *Biogeochemistry*
862 *of Seasonally Snow-Covered Catchments, IAHS pub. no.,* 228: 44-49.

863 Albert, M. R., Grannas, A. M., Bottenheim, J., Shepson, P. B., and Perron, F. E., 2002: Processes and
864 properties of snow-air transfer in the high Arctic with application to interstitial ozone at Alert,
865 Canada. *Atmospheric Environment,* 36: 2779-2787.
866 Allegrini, I., Ianniello, A., Montagnoli, M., Sparapani, R., Mazziotti Gomez de Teran, C., 1999: Carbon-
867 coated annular denuders and ion chromatographic measurements for the determination of
868 nitrogen-containing species (NO_2 and NO_y) in remote atmospheres. *Journal of Chromatography*
869 *A*, 846: 265–268.
870
871 Amato, P., Hennebelle, R., Magand, O., Sancelme, M., Delort, A. M., Barbante, C., Boutron, C., and
872 Ferrari, C., 2007: Bacterial characterization of the snow cover at Spitzberg, Svalbard. *Fems*
873 *Microbiology Ecology,* 59: 255-264.
874 Amoroso, A., Beine, H. J., Sparapani, R., Nardino, M., and Allegrini, I., 2006: Observation of coinciding
875 arctic boundary layer ozone depletion and snow surface emissions of nitrous acid. *Atmospheric*
876 *Environment,* 40: 1949-1956.
877 Amoroso, A., Domine, F., Esposito, G., Morin, S., Savarino, J., Nardino, M., Montagnoli, M., Bonneville,
878 J. M., Clement, J. C., Ianniello, A., and Beine, H. J., 2010: Microorganisms in Dry Polar Snow
879 Are Involved in the Exchanges of Reactive Nitrogen Species with the Atmosphere.
880 *Environmental Science & Technology,* 44: 714-719.
881 Avallone, L. M., Toohey, D. W., Fortin, T. J., McKinney, K. A., and Fuentes, J. D., 2003: In situ
882 measurements of bromine oxide at two high-latitude boundary layer sites: Implications of
883 variability. *Journal of Geophysical Research-Atmospheres,* 108.
884 Bartels-Rausch, T., Jacobi, H.-W., Kahan, T. F., Thomas, J. L., Thomson, E. S., Abbatt, J. P. D.,
885 Ammann, M., Blackford, J. R., Bluhm, H., Boxe, C., Domine, F., Frey, M. M., Gladich, I.,
886 Guzmán, M. I., Heger, D., Huthwelker, Th., Klán, P., Kuhs, W. F., Kuo, M. H., Maus, S., Moussa,
887 S. G., McNeill, V. F., Newberg, J. T., Pettersson, J. B. C., Roeselová, M., and Sodeau, J. R, 2012:
888 A review of air-ice chemical and physical interactions (AICI): liquids, quasi-liquids, and solids in
889 snow. *Atmospheric Chemistry and Physics*, 14: 1587-1633.
890 Barrie, L. and Platt, U., 1997: Arctic tropospheric chemistry: an overview. *Tellus Series B-Chemical and*
891 *Physical Meteorology,* 49: 450-454.
892 Barrie, L., Falck, E., Gregor, D. J., Iversen, T., Loeng, H., Macdonald, R., Pfirman, S., Skotvold, T., and
893 E., W., 1998: The Influence of Physical and Chemical Processes on Contaminant Transport into
894 and within the Arctic. *In* Gregor, D. J., Loeng, H., and Barrie, L. (eds.), *AMAP Assessment Report:*
895 *Arctic Pollution Issues*. Oslo: Arctic Monitoring and Assessment Programme (AMAP), 25-116.
896 Begoin, M., Richter, A., Weber, M., Kaleschke, L., Tian-Kunze, X., Stohl, A., Theys, N., and
897 Burrows, J. P., 2010: Satellite observations of long range transport of a large BrO plume in the
898 Arctic, *Atmospheric Chemistry and Physics*, 10: 6515-6526.
899 Beine, H. J., Engardt, M., Jaffe, D. A., Hov, Ø., Holmén, K., and Stordal, F., 1996: Measurements of NO_x
900 and aerosol particles at Ny-Ålesund Zeppelin mountain station on Svalbard: influence of regional
901 and local pollution sources. *Atmospheric Environment*, 30: 1067-1079.
902 Beine, H., Colussi, A. J., Amoroso, A., Esposito, G., Montagnoli, M., and Hoffmann, M. R., 2008:
903 HONO emissions from snow surfaces. *Environmental Research Letters,* 3.
904 Beine, H. J., Jaffe, D. A., Herring, J. A., Kelley, J. A., Krognes, T., and Stordal, F., 1997: High-latitude
905 springtime photochemistry. Part 1. NO_x, PAN and ozone relationships. *Journal of Atmospheric*
906 *Chemistry,* 27: 127-153.
907 Beine, H. J., Allegrini, I., Sparapani, R., Ianniello, A., and Valentini, F., 2001: Three years of springtime
908 trace gas and particle measurements at Ny-Alesund, Svalbard. *Atmospheric Environment,* 35:
909 3645-3658.

910 Beine, H. J., Domine, F., Simpson, W., Honrath, R. E., Sparapani, R., Zhou, X. L., and King, M., 2002a:
911 Snow-pile and chamber experiments during the Polar Sunrise Experiment 'Alert 2000':
912 exploration of nitrogen chemistry. *Atmospheric Environment,* 36: 2707-2719.
913 Beine, H. J., Honrath, R. E., Domine, F., Simpson, W. R., and Fuentes J. D., 2002b: NO_x during
914 background and ozone depletion periods at Alert: Fluxes above the snow surface: *Journal of*
915 *Geophysical Research*, 107(D21): 4584.
916 Beine, H. J., Domine, F., Ianniello, A., Nardino, M., Allegrini, I., Teinilä, K., and Hillamo, R., 2003:
917 Fluxes of nitrates between snow surfaces and the atmosphere in the European high Arctic.
918 *Atmospheric Chemistry and Physics,* 3: 335-346.
919 Bergin, M. H., Jaffrezo, J. L., Davidson, C. I., Dibb, J. E., Pandis, S. N., Hillamo, R., Maenhaut, W.,
920 Kuhns, H. D., and Makela, T., 1995: The Contributions of Snow, Fog, and Dry Deposition to the
921 Summer Flux of Anions and Cations at Summit, Greenland. *Journal of Geophysical Research-*
922 *Atmospheres,* 100: 16275-16288.
923 Björkman, M. P., Kühnel, R., Partridge, D. G., Roberts, T. J., Aas, W., Mazzola, M., Viola, A., Hodson,
924 A., Ström, J., and Isaksson, E., 2013: Nitrate dry deposition in Svalbard. *Tellus B,* 65.
925 Blunier, T., Floch, G. L., Jacobi, H. W., and Quansah, E., 2005: Isotopic view on nitrate loss in Antarctic
926 surface snow. *Geophysical Research Letters,* 32.
927 Boxe, C. S. and Saiz-Lopez, A., 2008: Multiphase modeling of nitrate photochemistry in the quasi-liquid
928 layer (QLL): implications for NO_x release from the Arctic and coastal Antarctic snowpack.
929 *Atmospheric Chemistry and Physics,* 8: 4855-4864.
930 Brooks, P. D., Schmidt, S. K., and Williams, M. W., 1997: Winter production of CO_2 and N_2O from
931 Alpine tundra: Environmental controls and relationship to inter-system C and N fluxes.
932 *Oecologia,* 110: 403-413.
933 Cadle, S. H., Dasch, J. M., and Mulawa, P. A., 1985: Atmospheric Concentrations and the Deposition
934 Velocity to Snow of Nitric-Acid, Sulfur-Dioxide and Various Particulate Species. *Atmospheric*
935 *Environment,* 19: 1819-1827.
936 Cadle, S. H., 1991: Dry Deposition to Snowpacks. *In* Davies, T. D., Tranter, M., and Jones, H. G. (eds.),
937 *Seasonal Snowpacks*. Berlin: Springer-Verlag, 21-66.
938 Chu, L. and Anastasio, C., 2003: Quantum yields of hydroxyl radical and nitrogen dioxide from the
939 photolysis of nitrate on ice. *Journal of Physical Chemistry A,* 107: 9594-9602.
940 Colbeck, S. C., 1997: Model of wind pumping for layered snow. *Journal of Glaciology,* 43: 60-65.
941 Coplen, T. B., Bohke, J. K., and Casciotti, K. L., 2004: Using dual-bacterial denitrification to improve
942 δ^{15}N determinations of nitrates containing mass-independent ^{17}O. *Rapid Communications in Mass*
943 *Spectrometry,* 18: 245-250.
944 Cress, R. G., Williams, M. W., and Sievering, H., 1995: Dry depositional loading of nitrogen to an alpine
945 snowpack, Niwot Ridge, Colorado, *Biogeochemistry of Seasonally Snow-Covered Catchments*:
946 IAHS Publ. no. 228, 33-40.
947 Dentener, F. J. and Crutzen, P. J., 1993: Reaction of N_2O_5 on Tropospheric Aerosols - Impact on the
948 Global Distributions of NO_x, O_3, and OH. *Journal of Geophysical Research-Atmospheres,* 98:
949 7149-7163.
950 Dibb, J. E., Talbot, R. W., Munger, J. W., Jacob, D. J., and Fan, S. M., 1998: Air-snow exchange of
951 HNO_3 and NO_y at Summit, Greenland. *Journal of Geophysical Research-Atmospheres,* 103:
952 3475-3486.
953 Dickerson, R. R., 1985: Reactive Nitrogen-Compounds in the Arctic. *Journal of Geophysical Research-*
954 *Atmospheres,* 90: 10739-10743.
955 Diehl, K., Mitra, S. K., and Pruppacher, H. R., 1995: A laboratory study of the uptake of HNO_3 and HCL
956 vapor by snow crystals and ice spheres at temperatures netween 0 and -40°C. *Atmospheric*
957 *Environment,* 29: 975-981.
958 Domine, F. and Shepson, P. B, 2002: Air-snow interactions and atmospheric chemistry. *Science*, 297:
959 1506-1510.

960 Domine, F., Albert, M., Huthwelker, T., Jacobi, H. W., Kokhanovsky, A. A., Lehning, M., Picard, G., and
961 Simpson, W. R., 2008: Snow physics as relevant to snow photochemistry. *Atmospheric Chemistry*
962 *and Physics,* 8: 171-208.
963 Elliott, E. M., Kendall, C., Boyer, E. W., Burns, D. A., Lear, G. G., Golden, H. E., Harlin, K.,
964 Bytnerowicz, A., Butler, T. J., and Glatz, R., 2009: Dual nitrate isotopes in dry deposition: Utility
965 for partitioning NOx source contributions to landscape nitrogen deposition. *Journal of*
966 *Geophysical Research-Biogeosciences,* 114.
967 Erbland, J., Vicars, W. C., Savarino, J., Morin, S., Frey, M. M., Frosini, D., Vince, E., and Martins, J. M.
968 F., 2013: Air-snow transfer of nitrate on the East Antarctic Plateau – Part 1: Isotopic evidence for
969 a photolytically driven dynamic equilibrium. *Atmospheric Chemistry and Physics* 13: 6403-6419.
970 Evans, M. J., Jacob, D. J., Atlas, E., Cantrell, C. A., Eisele, F., Flocke, F., Fried, A., Mauldin, R. L.,
971 Ridley, B. A., Wert, B., Talbot, R., Blake, D., Heikes, B., Snow, J., Walega, J., Weinheimer, A. J.,
972 and Dibb, J., 2003: Coupled evolution of BrO_x-ClO_x-HO_x-NO_x chemistry during bromine-
973 catalyzed ozone depletion events in the arctic boundary layer. *Journal of Geophysical Research-*
974 *Atmospheres,* 108.
975 Febo, A., Desantis, F., Perrino, C., and Giusto, M., 1989: Evaluation of laboratory and field performance
976 of denuder tubes - a theoretical approach. *Atmospheric Environment,* 23: 1517-1530.
977 Felix, J. D. and Elliott, E. M., 2013: The agricultural history of human-nitrogen interactions as recorded
978 in ice core $\delta^{15}N$-NO_3^-. *Geophysical Research Letters,* 40: 1642-1646.
979 Foster, K. L., Plastridge, R. A., Bottenheim, J. W., Shepson, P. B., Finlayson-Pitts, B. J., and Spicer, C.
980 W., 2001: The role of Br_2 and BrCl in surface ozone destruction at polar sunrise. *Science,* 291:
981 471-474.
982 France, J. L., King, M. D., and Lee-Taylor, J., 2010: The importance of considering depth-resolved
983 photochemistry in snow: a radiative-transfer study of NO_2 and OH production in Ny-Alesund
984 (Svalbard) snowpacks. *Journal of Glaciology,* 56: 655-663.
985 France, J. L., King, M. D., Frey, M. M., Erbland, J., Picard, G., Preunkert, S., MacArthur, A., and
986 Savarino, J., 2011a: Snow optical properties at Dome C (Concordia), Antarctica; implications for
987 snow emissions and snow chemistry of reactive nitrogen. *Atmospheric Chemistry and Physics,* 11:
988 9787-9801.
989 France, J. L., King, M. D., Lee-Taylor, J., Beine, H. J., Ianniello, A., Domine, F., and MacArthur, A.,
990 2011b: Calculations of in-snow NO_2 and OH radical photochemical production and photolysis
991 rates: A field and radiative-transfer study of the optical properties of Arctic (Ny-Alesund,
992 Svalbard) snow. *Journal of Geophysical Research-Earth Surface,* 116.
993 Frey, M. M., Stewart, R. W., McConnell, J. R., and Bales, R. C., 2005: Atmospheric hydroperoxides in
994 West Antarctica: Links to stratospheric ozone and atmospheric oxidation capacity. *Journal of*
995 *Geophysical Research-Atmospheres,* 110.
996 Frey, M. M., Savarino, J., Morin, S., Erbland, J., and Martins, J. M. F., 2009: Photolysis imprint in the
997 nitrate stable isotope signal in snow and atmosphere of East Antarctica and implications for
998 reactive nitrogen cycling. *Atmospheric Chemistry and Physics,* 9: 8681-8696.
999 Freyer, H. D., 1991: Seasonal variation of $^{15}N/^{14}N$ ratios in atmospheric nitrate species. *Tellus Series B-*
1000 *Chemical and Physical Meteorology,* 43: 30-44.
1001 Galbavy, E. S., Anastasio, C., Lefer, B., and Hall, S., 2007: Light penetration in the snowpack at Summit,
1002 Greenland: Part 2 nitrate photolysis. *Atmospheric Environment,* 41: 5091-5100.
1003 Grannas, A. M., Jones, A. E., Dibb, J., Ammann, M., Anastasio, C., Beine, H. J., Bergin, M., Bottenheim,
1004 J., Boxe, C. S., Carver, G., Chen, G., Crawford, J. H., Domine, F., Frey, M. M., Guzman, M. I.,
1005 Heard, D. E., Helmig, D., Hoffmann, M. R., Honrath, R. E., Huey, L. G., Hutterli, M., Jacobi, H.
1006 W., Klan, P., Lefer, B., McConnell, J., Plane, J., Sander, R., Savarino, J., Shepson, P. B.,
1007 Simpson, W. R., Sodeau, J. R., von Glasow, R., Weller, R., Wolff, E. W., and Zhu, T., 2007: An
1008 overview of snow photochemistry: evidence, mechanisms and impacts. *Atmospheric Chemistry*
1009 *and Physics,* 7: 4329-4373.

1010 Hanson, D. R. and Ravishankara, A. R., 1995: Heterogeneous Chemistry of Bromine Species in Sulfuric-
1011 Acid under Stratospheric Conditions. *Geophysical Research Letters,* 22: 385-388.
1012 Hanson, D. R., Ravishankara, A. R., and Lovejoy, E. R., 1996: Reaction of $BrONO_2$ with H_2O on
1013 submicron sulfuric acid aerosol and the implications for the lower stratosphere. *Journal of*
1014 *Geophysical Research-Atmospheres,* 101: 9063-9069.
1015 Hastings, M. G., Steig, E. J., and Sigman, D. M., 2004: Seasonal variations in N and O isotopes of nitrate
1016 in snow at Summit, Greenland: Implications for the study of nitrate in snow and ice cores.
1017 *Journal of Geophysical Research-Atmospheres,* 109.
1018 Hastings, M. G., 2010: Evaluating source, chemistry and climate change based upon the isotopic
1019 composition of nitrate in ice cores. *IOP Conference Series: Earth and Environmental Science,* 9:
1020 012002.
1021 Hirdman, D., Sodemann, H., Eckhardt, S., Burkhart, J. F., Jefferson, A., Mefford, T., Quinn, P. K.,
1022 Sharma, S., Ström, J., and Stohl, A., 2010: Source identification of short-lived air pollutants in
1023 the Arctic using statistical analysis of measurement data and particle dispersion model output.
1024 *Atmospheric Chemistry and Physics,* 10: 669-693.
1025 Hodson, A. J., Mumford, P. N., Kohler, J., and Wynn, P. M., 2005: The High Arctic glacial ecosystem:
1026 new insights from nutrient budgets. *Biogeochemistry,* 72: 233-256.
1027 Hodson, A. J., Roberts T. J., Engvall A.-C., Holmén K., Mumford P., 2010: Glacier ecosystem response
1028 to episodic nitrogen enrichment in Svalbard, European High Arctic. *Biogeochemistry*, 98, 1-3,
1029 171-184. Honrath, R. E., Peterson, M. C., Guo, S., Dibb, J. E., Shepson, P. B., and Campbell, B.,
1030 1999: Evidence of NO_x production within or upon ice particles in the Greenland snowpack.
1031 *Geophysical Research Letters,* 26: 695-698.
1032 Honrath, R. E., Peterson, M. C., Dziobak, M. P., Dibb, J. E., Arsenault, M. A., and Green, S. A., 2000:
1033 Release of NO_x from sunlight-irradiated midlatitude snow. *Geophysical Research Letters,* 27:
1034 2237-2240.
1035 Hopper, J. F., Peters, B., Yokouchi, Y., Niki, H., Jobson, B. T., Shepson, P. B., and Muthuramu, K., 1994:
1036 Chemical and meteorological observations at ice camp swan during polar sunrise experiment
1037 1992. *Journal of Geophysical Research-Atmospheres,* 99: 25489-25498.
1038 Hopper, J. F., Barrie, L. A., Silis, A., Hart, W., Gallant, A. J., and Dryfhout, H., 1998: Ozone and
1039 meteorology during the 1994 Polar Sunrise Experiment. *Journal of Geophysical Research-*
1040 *Atmospheres,* 103: 1481-1492.
1041 Huff, D. M., Joyce, P. L., Fochesatto, G. J., and Simpson, W. R., 2011: Deposition of dinitrogen
1042 pentoxide, N_2O_5, to the snowpack at high latitudes. *Atmospheric Chemistry and Physics,* 11:
1043 4929-4938.
1044 Ianniello, A., Beine, H. J., Sparapani, R., Di Bari, F., Allegrini, I., and Fuentes, J. D., 2002: Denuder
1045 measurements of gas and aerosol species above Arctic snow surfaces at Alert 2000. *Atmospheric*
1046 *Environment,* 36: 5299-5309.
1047 Ianniello, A., Beine, H. J., Landis, M. S., Stevens, R. K., Esposito, G., Arnoroso, A., and Allegrini, I.,
1048 2007: Comparing field performances of denuder techniques in the high Arctic. *Atmospheric*
1049 *Environment,* 41: 1604-1615.
1050 Ianniello, A., Spataro, F., Esposito, G., Allegrini, I., Hu, M., and Zhu, T., 2011: Chemical characteristics
1051 of inorganic ammonium salts in PM2.5 in the atmosphere of Beijing (China). *Atmospheric*
1052 *Chemistry and Physics,* 11: 10803-10822.
1053 Jacobi, H. W. and Hilker, B., 2007: A mechanism for the photochemical transformation of nitrate in snow.
1054 *Journal of Photochemistry and Photobiology a-Chemistry,* 185: 371-382.
1055 Jacobi, H. W., Morin, S., and Bottenheim, J. W., 2010: Observation of widespread depletion of ozone in
1056 the springtime boundary layer of the central Arctic linked to mesoscale synoptic conditions.
1057 *Journal of Geophysical Research-Atmospheres,* 115: D17302.

Jacobi, H. W., Kleffmann, J., Villena, G., Wiesen, P., King. M., France, J., Anastasio, C., and Staebler, R., 2014: Role of Nitrate in the Photochemical Formation of Radicals in the Snow. *Environmental Science and Technology*, 48:165-172.

Jarvis, J. C., Steig, E. J., Hastings, M. G., and Kunasek, S. A., 2008: Influence of local photochemistry on isotopes of nitrate in Greenland snow. *Geophysical Research Letters,* 35.

Jarvis, J. C., Hastings, M. G., Steig, E. J., and Kunasek, S. A., 2009: Isotopic ratios in gas-phase HNO_3 and snow nitrate at Summit, Greenland. *Journal of Geophysical Research-Atmospheres,* 114: -.

Johansson, C. and Granat, L., 1986: An Experimental-Study of the Dry Deposition of Gaseous Nitric-Acid to Snow. *Atmospheric Environment,* 20: 1165-1170.

Jones, A. E., Weller, R., Wolff, E. W., and Jacobi, H. W., 2000: Speciation and rate of photochemical NO and NO_2 production in Antarctic snow. *Geophysical Research Letters,* 27: 345-348.

Jones, A. E., Weller, R., Anderson, P. S., Jacobi, H. W., Wolff, E. W., Schrems, O., and Miller, H., 2001: Measurements of NO_x emissions from the Antarctic snowpack. *Geophysical Research Letters,* 28: 1499-1502.

Kaiser, J., Hastings, M. G., Houlton, B. Z., Rockmann, T., and Sigman, D. M., 2007: Triple oxygen isotope analysis of nitrate using the denitrifier method and thermal decomposition of N_2O. *Analytical Chemistry,* 79: 599-607.

Kendall, C., 1998: Tracing Nitrogen Sources and Cycling in Catchments. *In* Kendall, C. and McDonnell, J. J. (eds.), *Isotope Tracers in Catchment Hydrology*. Amsterdam: Elsevier Science B.V., 839pp.

Kendall, C., Elliott, E. M., and Wankel, S. D., 2007: Tracing anthropogenic inputs of nitrogen to ecosystems. *In* Michener, R. H. and Lajtha, K. (eds.), *Stable Isotopes in Ecology and Environmental Science*: Blackwell Publishing, 375-449.

Kuhn, M., 2001: The nutrient cycle through snow and ice, a review. *Aquatic Sciences,* 63: 150-167.

Kvlividz, V. I., Kiselev, V. F., and Ushakova, L. A., 1970: Existence of Quasi-Liquid Layer on Ice Surface (*in Russian*). *Doklady Akademii Nauk Sssr,* 191: 1088-1090.

Kühnel, R., Roberts, T. J., Björkman, M. P., Isaksson, E., Aas, W., Holmén, K., and Ström, J., 2011: 20-Year Climatology of NO_3^- and NH_4^+ Wet Deposition at Ny-Ålesund, Svalbard. *Advances in Meteorology,* 2011: 10.

Kühnel, R., 2013: Reactive Nitrogen: Transport to and deposition at the high Arctic site Ny-Ålesund, Svalbard, 236 pp, University of Oslo, Oslo.

Larose, C., Berger, S., Ferrari, C., Navarro, E., Dommergue, A., Schneider, D., and Vogel, T. M., 2010: Microbial sequences retrieved from environmental samples from seasonal Arctic snow and meltwater from Svalbard, Norway. *Extremophiles,* 14: 205-212.

Ma, W. K., Schautz, A., Fishback, L. A. E., Bedard-Haughn, A., Farrell, R. E., and Siciliano, S. D., 2007: Assessing the potential of ammonia oxidizing bacteria to produce nitrous oxide in soils of a high arctic lowland ecosystem on Devon Island, Canada. *Soil Biology & Biochemistry,* 39: 2001-2013.

McCabe, J. R., Boxe, C. S., Colussi, A. J., Hoffmann, M. R., and Thiemens, M. H., 2005: Oxygen isotopic fractionation in the photochemistry of nitrate in water and ice. *Journal of Geophysical Research-Atmospheres,* 110: D15310.

Michalski, G., Scott, Z., Kabiling, M., and Thiemens, M. H., 2003: First measurements and modeling of $\Delta^{17}O$ in atmospheric nitrate. *Geophysical Research Letters,* 30.

Miteva, V., 2008: *Bacteria in snow and glacier ice*: Springer-Verlag Berlin, Heidelberger Platz 3, D-14197 Berlin, Germany, 31-50.

Morin, S., Savarino, J., Bekki, S., Cavender, A., Shepson, P. B., and Bottenheim, J. W., 2007a: Major influence of BrO on the NO_x and nitrate budgets in the Arctic spring, inferred from $\Delta^{17}O(NO_3^-)$ measurements during ozone depletion events. *Environmental Chemistry,* 4: 238-241.

Morin, S., Savarino, J., Bekki, S., Gong, S., and Bottenheim, J. W., 2007b: Signature of Arctic surface ozone depletion events in the isotope anomaly (Delta O-17) of atmospheric nitrate. *Atmospheric Chemistry and Physics,* 7: 1451-1469.

1107 Morin, S., Savarino, J., Frey, M. M., Yan, N., Bekki, S., Bottenheim, J. W., and Martins, J. M. F., 2008:
1108 Tracing the Origin and Fate of NO_x in the Arctic Atmosphere Using Stable Isotopes in Nitrate.
1109 *Science,* 322: 730-732.
1110 Morin, S., Savarino, J., Frey, M. M., Domine, F., Jacobi, H. W., Kaleschke, L., and Martins, J. M. F.,
1111 2009: Comprehensive isotopic composition of atmospheric nitrate in the Atlantic Ocean boundary
1112 layer from 65 degrees S to 79 degrees N. *Journal of Geophysical Research-Atmospheres,* 114:
1113 D05303.
1114 Perrino, C., Ramirez, D., and Allegrini, I., 2001: Monitoring acidic air pollutants near Rome by means of
1115 diffusion lines: development of a specific quality control procedure. *Atmospheric Environment,*
1116 35: 331-341.
1117 Qiu, R., Green, S. A., Honrath, R. E., Peterson, M. C., Lu, Y., and Dziobak, M., 2002: Measurements of
1118 J_{NO3-} in snow by nitrate-based actinometry. *Atmospheric Environment,* 36: 2563-2571.
1119 Rahn, K. A., Joranger, E., Semb, A., and Conway, T. J., 1980: High Winter Concentrations of SO_2 in the
1120 Norwegian Arctic and Transport from Eurasia. *Nature,* 287: 824-826.
1121 Rahn, K. A., 1981: Relative importances of North-America and Eurasia as sources of Arctic aerosol.
1122 *Atmospheric Environment,* 15: 1447-1455.
1123 Roberts T. J., Hodson A., Evans C. D., Holmén, K., 2010: Modelling the impacts of a nitrogen pollution
1124 event on the biogeochemistry of an Arctic glacier. Annals of Glaciology, 51: 163-170.
1125 Russell, A. G., Mcrae, G. J., and Cass, G. R., 1985: The Dynamics of Nitric-Acid Production and the Fate
1126 of Nitrogen-Oxides. *Atmospheric Environment,* 19: 893-903.
1127 Sander, R. and Bottenheim, J., 2012: A compilation of tropospheric measurements of gas-phase and
1128 aerosol chemistry in polar regions. *Earth System Science Data*, 4: 215–282.
1129 Sato, K., Takenaka, N., Bandow, H., and Maeda, Y., 2008: Evaporation loss of dissolved volatile
1130 substances from ice surfaces. *Journal of Physical Chemistry A,* 112: 7600-7607.
1131 Seinfeld, J. H. and Pandis, S. N., 2006: *Atmosperic Chemistry and Physics: From Air Pollution to*
1132 *Climate Change, Second Edition*. Hoboken, New Jersey: John Wiley & sons, Inc.
1133 Siciliano, S. D., Ma, W. K., Ferguson, S., and Farrell, R. E., 2009: Nitrifier dominance of Arctic soil
1134 nitrous oxide emissions arises due to fungal competition with denitrifiers for nitrate. *Soil Biology*
1135 *& Biochemistry,* 41: 1104-1110.
1136 Sigman, D. M., Casciotti, K. L., Andreani, M., Barford, C., Galanter, M., and Bohlke, J. K., 2001: A
1137 bacterial method for the nitrogen isotopic analysis of nitrate in seawater and freshwater.
1138 *Analytical Chemistry,* 73: 4145-4153.
1139 Simpson, W. R., King, M. D., Beine, H. J., Honrath, R. E., and Zhou, X. L., 2002: Radiation-transfer
1140 modeling of snow-pack photochemical processes during ALERT 2000. *Atmospheric Environment,*
1141 36: 2663-2670.
1142 Simpson, W. R., von Glasow, R., Riedel, K., Anderson, P., Ariya, P., Bottenheim, J., Burrows, J.,
1143 Carpenter, L. J., Friess, U., Goodsite, M. E., Heard, D., Hutterli, M., Jacobi, H. W., Kaleschke, L.,
1144 Neff, B., Plane, J., Platt, U., Richter, A., Roscoe, H., Sander, R., Shepson, P., Sodeau, J., Steffen,
1145 A., Wagner, T., and Wolff, E., 2007: Halogens and their role in polar boundary-layer ozone
1146 depletion. *Atmospheric Chemistry and Physics,* 7: 4375-4418.
1147 Sozzi, R., Favaron, M., Georgiadis, T., 1998: Method for estimation of surface roughness and similarity
1148 function of wind speed vertical profile. *Journal of Applied Meteorology*, 37: 461–469.
1149 Spataro, F., Ianniello, A., Esposito, G., Allegrini, I., Zhu, T., and Hu, M., 2013: Occurrence of
1150 atmospheric nitrous acid in the urban area of Beijing (China). *Science of the Total Environment,*
1151 447: 210-224.
1152 Stohl, A., 2006: Characteristics of atmospheric transport into the Arctic troposphere. *Journal of*
1153 *Geophysical Research-Atmospheres,* 111: D11306.
1154 Sturm, M. and Johnson, J. B., 1991: Natural-Convection in the Sub-Arctic Snow Cover. *Journal of*
1155 *Geophysical Research-Solid Earth and Planets,* 96: 11657-11671.

1156 Thomas, J. L., Stutz, J., Lefer, B., Huey, L. G., Toyota, K., Dibb, J. E., and von Glasow, R., 2011:
1157 Modeling chemistry in and above snow at Summit, Greenland - Part 1: Model description and
1158 results. *Atmospheric Chemistry and Physics,* 11: 4899-4914.
1159 Thomas, J. L., Dibb, J. E., Huey, L. G., Liao, J., Tanner, D., Lefer, B., von Glasow, R., and Stutz, J., 2012:
1160 Modeling chemistry in and above snow at Summit, Greenland - Part 2: Impact of snowpack
1161 chemistry on the oxidation capacity of the boundary layer. *Atmospheric Chemistry and Physics,*
1162 12: 6537-6554.
1163 Vega, C. P., 2014: Nitrate stable isotopes and major ions in snow and ice from Svalbard, 80 pp, Uppsala
1164 University, Uppsala.
1165 Villena, G., Wiesen, P., Cantrell, C. A., Flocke, F., Fried, A., Hall, S. R., Hornbrook, R. S., Knapp, D.,
1166 Kosciuch, E., Mauldin III, R. L., McGrath, J. A., Montzka, D., Richter, D., Ullmann, K., Walega,
1167 J., Weibring, P., Weinheimer, A., Staebler, R. M., Liao, J., Huey, L. G., and Kleffmann, J., 2011:
1168 Nitrous acid (HONO) during polar spring in Barrow, Alaska: A net source of OH radicals?
1169 *Journal of Geophysical Research*, 116: D00R07.
1170 Zhou, X. L., Beine, H. J., Honrath, R. E., Fuentes, J. D., Simpson, W., Shepson, P. B., and Bottenheim, J.
1171 W., 2001: Snowpack photochemical production of HONO: a major source of OH in the Arctic
1172 boundary layer in springtime. *Geophysical Research Letters,* 28: 4087-4090.
1173 Zien, A. W., Richter, A., Hilboll, A., Blechschmidt, A.-M., and Burrows, J. P., 2014: Systematic analysis
1174 of tropospheric NO_2 long-range transport events detected in GOME-2 satellite data. *Atmospheric*
1175 *Chemistry and Physics*, 14: 7367-7396.

1176 Table 1. Fitted linear regression models (y=*k*x+*m*) for the three periods (Fig. 4)*.

Model	Period	*k*	*m*	*n*	R^2	p-value	Unit
c_{NO3}	1	0.1	−7.8	30	0.17	< 0.03	µmol L^{-1}
	2	0.2	−18.1	12	0.50	0.01	µmol L^{-1}
	3	0.1	−6.5	26	0.34	< 0.01	µmol L^{-1}
c_{Br}	1	1.5	−61.3	29	0.06	0.18	nmol L^{-1}
	2	−20.6	2100.4	12	0.56	< 0.01	nmol L^{-1}
	3	−4.5	566.2	23	0.56	<< 0.01	nmol L^{-1}
c_{Cl}	1	2.4	−206.6	29	0.09	0.11	µmol L^{-1}
	2	3.4	−348.0	12	0.04	0.56	µmol L^{-1}
	3	3. 1	−339.7	26	0.45	< 0.01	µmol L^{-1}
c_{Na}	1	1.0	−70.8	30	0.02	0.42	µmol L^{-1}
	2	2.7	−279.4	12	0.06	0.43	µmol L^{-1}
	3	3.2	−354.8	27	0.40	< 0.01	µmol L^{-1}
$\delta(^{15}N)$	1	−0.1	8.8	23	0.01	0.67	‰
	2	−0.4	41.6	12	0.02	0.65	‰
	3	0.6	−85.1	26	0.49	< 0.01	‰
$\delta(^{18}O)$	1	−0.1	90.2	23	0.00	0.78	‰
	2	0.9	−20.7	12	0.28	0.08	‰
	3	0.7	−0.4	26	0.37	< 0.01	‰
z_{SWE}	1	0.1	−8.2	30	0.50	<< 0.01	cm
	2	0.03	−2.0	12	0.02	0.63	cm
	3	0.2	−21.1	26	0.88	<< 0.01	cm
V	1	4.0	−346.8	30	0.50	<< 0.01	mL
	2	−0.7	−157.3	12	0.01	0.80	mL
	3	7. 8	−896.6	26	0.88	<< 0.01	mL

1177 *Regression models where analyzed for the NO_3^- concentration (c_{NO3}), Br^- concentration (c_{Br}),
1178 Cl^- concentration (c_{Cl}), Na^+ concentration (c_{Na}), the NO_3^- isotopic composition ($\delta(^{15}N)$ and
1179 $\delta(^{18}O)$), the surface snow water equivalence (z_{SWE}), and the sample volume (V). Also given are
1180 the numbers of measurements (n) used for each regression, the multiple R^2 value for the models,
1181 and the significance (p-value) of the slope k.

1182 Table 2. Calculated initial ($_0$) and final ($_t$) values from the regression model in Table 1.

Model	Period	$_0$	$_t$	Unit
c_{NO3}	1	1.1±0.2	1.8±0.2	µmol L^{-1}
	2	1.4±0.1	1.9±0.1	µmol L^{-1}
	3	1.7±0.1	2.3±0.1	µmol L^{-1}
$\delta(^{15}N)$	1	−5.3±1.8	−6.5±1.7	‰
	2	−7.4±1.7	−8.7±1.7	‰
	3	−12.9±0.6	−8.0±0.6	‰
$\delta(^{18}O)$	1	84.0±1.2	83.4±1.2	‰
	2	85.2±0.9	88.0±0.9	‰
	3	83.0±0.9	88.7±0.9	‰
z_{SWE}	1	1.3±0.1	2.2±0.1	cm
	2	1.7±0.1	1.8±0.1	cm
	3	0.4±0.1	1.8±0.1	cm
V	1	57.2±4.0	92.9±4.0	mL
	2	73.4±5.2	71.2±5.2	mL
	3	15.6±2.9	78.0±2.9	mL

1183

1184 Table 3. Calculated net change of NO_3^- (F_{net}) and isotopic signatures ($\delta(^{15}N)$ and $\delta(^{18}O)$).

Period	$\boldsymbol{F_{net}}^*$ (μmol m^{-2} d^{-1})	$\boldsymbol{\delta(^{15}N)}^\#$ (‰)	$\boldsymbol{\delta(^{18}O)}^\#$ (‰)
1	0.9±0.4	−8.2±13.6	82.7±87.9
2	1.4±0.6	−12.2±18.8	95.4±110.6
3	0.6±0.2	7.0±5.6	105.9±72.3

1185 *calculated from Eq. 2
1186 #calculated from Eq. 5.
1187

Figure captions:

Figure 1. Maps of a) the Ny-Ålesund region and b) the Svalbard archipelago. Included in a) as a star is the surface snow sampling site and ”Gruvebadet” (a newly established research site), the Amundsen-Nobile Climate Change Tower (CCT) and the Zeppelin Station. In b) the most commonly used ice-core drilling sites (Holtedahlfonna, Lomonosovfonna and Austfonna) are given along with the major settlements (Longyearbyen, Barentsburg, Svea, Ny-Ålesund and Hornsund).

Figure 2. A schematic of the processes important for NO_3^- dynamics in Svalbard surface snow.

Figure 3. Nitrate concentrations (c_{NO3}) and isotopic signatures ($\delta(^{15}N)$ and $\delta(^{18}O)$) of the daily surface snow samples in 2010. Including; a) a schematic sketch of the visible layering found in the sampled surface snow; b) the atmospheric O_3 concentration (c_{O3}) measured at the Zeppelin Station and at Gruvebadet, along with surface snow Br^- concentrations (c_{Br}); c) a schematic sketch of 7 days back-trajectories obtained from the FLEXTRA model, where arrows indicate flow paths and circles indicate stagnant air; d) the measured $\delta(^{15}N)$ and $\delta(^{18}O)$ in the surface snow, and; e) the measured c_{NO3} in the surface snow together with the registered precipitation in Ny-Ålesund. Furthermore, error bars indicates standard error ($\sigma_{\bar{x}}$), * indicate samples where $\sigma_{\bar{x}}$ is calculated from only two data points, and symbols without error bars indicates one replicate. Solid lines represent significant linear regression models (lm, p-value < 0.05), while broken lines equal non-significant trends (p-value > 0.05).

Figure 4. Measured flux data (6 minute resolution) from Gruvebadet during the spring campaign 2010. Including; a) the NO concentrations (C_{NO}) at the upper and lower inlets; b) the NO_2 concentrations (C_{NO2}) at the upper and lower inlets; c) the NO and NO_2 flux data (F_{NO} and F_{NO2}, respectively) derived from the difference between the upper and lower inlets and the eddy diffusivity, *K*.

Figure 5. Measured and modelled NO_x, HNO_3 and p-NO_3^- fluxes measured at Gruvebadet. Where; a) is the photolytic rate (J_{NO3-}) estimated from Eq. 7; b) is the daily average emission and deposition of NO, NO_2 and NO_x (F_{NO}, F_{NO2} and F_{NOx}) and the daily NO_x net flux (ΣF_{NOx}). Also included is the estimated photolytic NO_2 flux (F_{JNO3-}) using J_{NO3-} in a) and the measured c_{NO3} in Fig. 3e; c) is the daily average emission and deposition of HNO_3 (F_{HNO3}) and p-NO_3^- ($F_{p\text{-}NO3}$) and the net flux of these (ΣF_{NO3}), also included is the measured (F_{tray}) and modelled (F_{model}(LND)) NO_3^- dry deposition to Ny-Ålesund given in Björkman et al. (2013).

Figure 6. Box model results, using the NO_x, HNO_3^- and p-NO_3^- flux measurements. Given in a) is the modeled δ_t for ^{18}O (Eq. 13) for the three isotopic deposition scenarios (δ_{atm}) where; + 40 ‰ resembles the OH signal found in Greenland (Jarvis et al., 2009); + 75 ‰ resembles a mid-latitude signal (Morin et al., 2009); and + 100 ‰ resembles the influence of BrO chemistry (Morin et al., 2009). Also included in a) is the actual measured $\delta(^{18}O)$ and co-occurring linear regression models (*lm,* Table 1). Similarly b) gives the modeled δ_t for ^{15}N (Eq. 13) for the three isotopic deposition scenarios (δ_{atm}) where; – 20 ‰ represents Polar basin air (Morin et al., 2009);

1232 – 13 ‰ represent ambient air (Amoroso et al., 2010); and + 5 ‰ represents a local
1233 biogeochemical signal (Amoroso et al.,2010). Also included in b) is the measured $\delta(^{15}N)$ and
1234 developed *lm*'s. Given in c) is the modeled c_t (Eq. 16) along with the measured c_{NO3} and *lm*'s.
1235 Furthermore, the fractionation sensitivity test is included as shaded areas around the box model
1236 results in a) and b).

1237 Figure 7. Same as Fig. 6 but where the box model parameterization for three mission of NO_x
1238 from the snow-pack is based on the photolytic rate function (J_{NO3-}, Eq. 7) and the deposition of
1239 nitrate from the atmosphere based on the dry deposition rate (F_{tray}) using Eq. 11 and 12.

1240

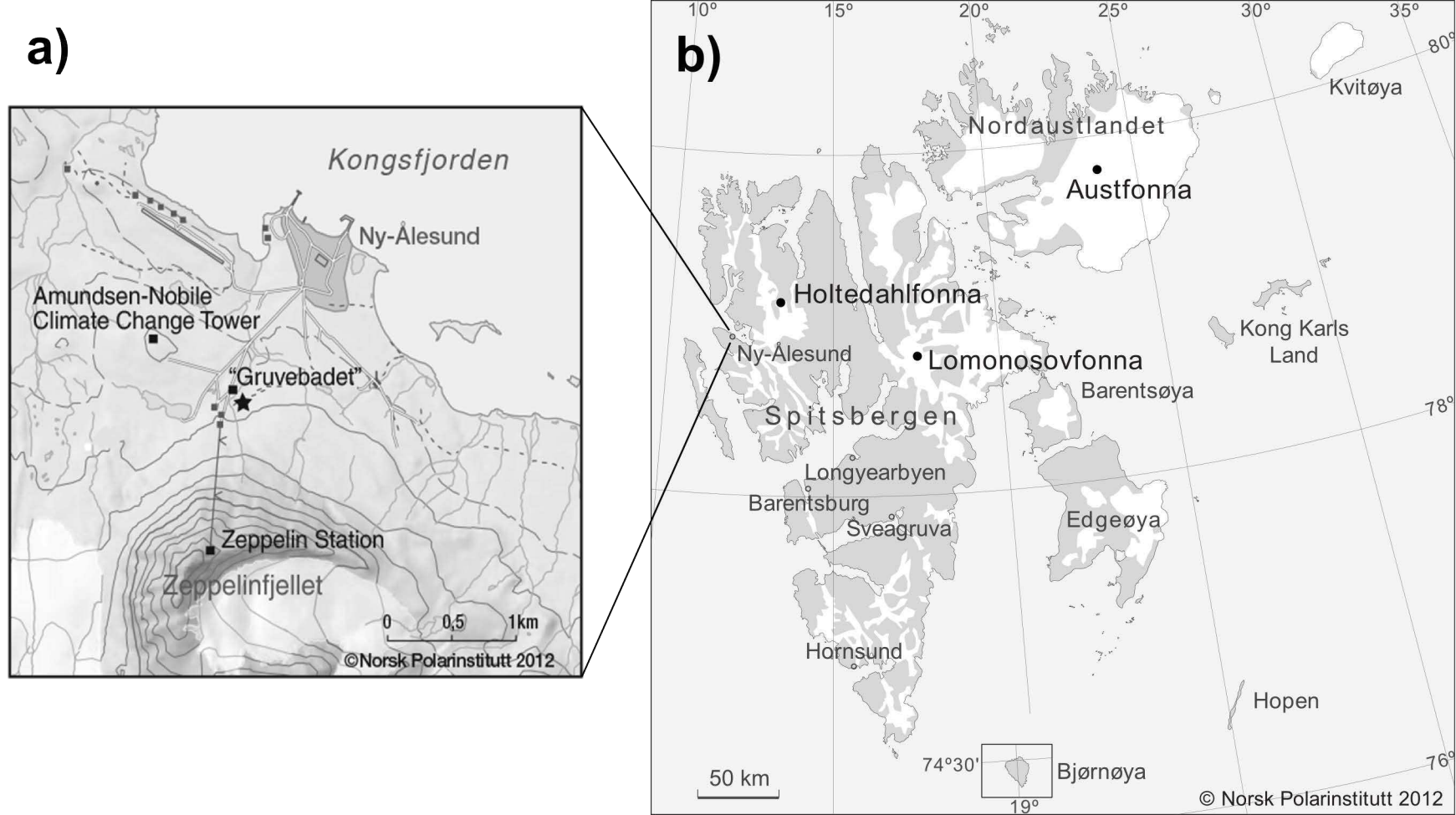
a)
Kongsfjorden
Ny-Ålesund
Amundsen-Nobile
Climate Change Tower
"Gruvebadet"
Zeppelin Station
Zeppelinfjellet
0 0,5 1km
©Norsk Polarinstitutt 2012
b)
10°
15°
20°
25°
30°
35°
80°
78°
76°
Kvitøya
Nordaustlandet
Austfonna
Holtedahlfonna
Ny-Ålesund
Lomonosovfonna
Kong Karls
Land
Barentsøya
Spitsbergen
Longyearbyen
Barentsburg
Sveagruva
Edgeøya
Hornsund
Hopen
74°30'
Bjørnøya
19°
50 km
© Norsk Polarinstitutt 2012

Long-range Atmospheric Transport

Atmosperic boundary layer

Snowpack interstitial air pockets

p-NO_3^-

PANs

NO_x

BrO-pathways

BrO

O_3

Br_2 *hv* Br *hv* BrO

hv

$BrONO_2$

NO_2

NO_3

hv

hv

hv

HOBr

H_2O(s)

NO_x-cycling

NO_2

O_3

XO_2, BrO

hv

NO

hv, *NO*

NO_x-removal

HO_2

HNO_4

M

O_3

NO_3

hv, NO

N_2O_5

HCHO

RCHO

H_2O(s)

X(aq)*

OH + *M*

HNO_3

HNO_3

H_2O

HNO_3(aq)

Dry Deposition

Wet Deposition

$Br^- + H^+$

hv

Snowpack

Biogeochemical cycling

NO_3^-

NO_2^-

HNO_3

NO

HONO

clay-NH_4^+

HNO_3

hv

evaporation

HONO

NO

O_2

hv

hv

OH

$NO_2 + H_2O$

hv

NO_2

OH

H_2O, $NO + H_2O$

NO_2^-

H^+

OH, H_2O

hv

hv, O

NO_3^-

H^+

Disorderd Interface (DI)

a)

b)

c) *Back trajectories*

d)

e)

period 1 *period 2* *period 3*

11 Feb 15 Feb 12 Apr 17 Apr 22 Apr 27 Apr 02 May 07 May

lm ($p < 0.05$) — c_{O_3} (Zeppelin) — $c_{NO_3^-}$ — $\delta(^{15}N)$ — Precipitation

lm ($p > 0.05$) — c_{O_3} (Gruvebadet) — c_{Br^-} — $\delta(^{18}O)$

a)

b)

c)

period 1

period 2

period 3

Emission

Deposition

C_{NO_2} (pmol mol^{-1})

C_{NO} (pmol mol^{-1})

F_{NO} & F_{NO_2} (pmol m^{-2} s^{-1})

160
120
80
40
0

40
20
10
0
-10
-20
-40

12 Apr
17 Apr
22 Apr
27 Apr
02 May
07 May

C_{NO_2}- upper
C_{NO}- upper
F_{NO}
C_{NO_2}- lower
C_{NO}- lower
F_{NO_2}

a)

b)

c)

J x 10^{-6} (s^{-1})

F_{NO_x} (μmol m^{-2} d^{-1})

$F_{NO_3^-}$ (μmol m^{-2} d^{-1})

0.12

0

2

1

0

-1

-2

1

0

-1

-2

-3

-4

period 1

period 2

period 3

Emission

Deposition

Emission

Deposition

$J_{NO_3^-}$

$F_{J_{NO_3^-}}$

F_{NO_x}

F_{NO}

F_{NO_2}

ΣF_{NO_x}

F_{tray}

F_{model}(LND)

F_{HNO_3}

$F_{p\text{-}NO_3}$

ΣF_{NO_3}

12 Apr

17 Apr

22 Apr

27 Apr

02 May

07 May

a)

δ_t & $\delta(^{18}O)$ (‰)

90
85
80
75

b)

δ_t & $\delta(^{15}N)$ (‰)

0
-5
-10
-15

c)

c_t & $c_{NO_3^-}$ (µmol L^{-1})

5
4
3
2
1
0

period 1

period 2

period 3

12 Apr
17 Apr
22 Apr
27 Apr
02 May
07 May

$\delta_{atm}(^{18}O)$ = +40 ‰
$\delta_{atm}(^{18}O)$ = +75 ‰
$\delta_{atm}(^{18}O)$ = +100 ‰
$\delta_{atm}(^{15}N)$ = -20 ‰
$\delta_{atm}(^{15}N)$ = -13 ‰
$\delta_{atm}(^{15}N)$ = +5 ‰
lm ($p < 0.05$)
lm ($p > 0.05$)
c_t (Eq. 16)

a)

δ_t & $\delta(^{18}O)$ (‰)

90
85
80
75

b)

δ_t & $\delta(^{15}N)$ (‰)

0
-5
-10
-15

c)

c_t & $c_{NO_3^-}$ (µmol L^{-1})

5
4
3
2
1
0

period 1

period 2

period 3

12 Apr
17 Apr
22 Apr
27 Apr
02 May
07 May

$\delta_{atm}(^{18}O)$ = +40 ‰
$\delta_{atm}(^{18}O)$ = +75 ‰
$\delta_{atm}(^{18}O)$ = +100 ‰
$\delta_{atm}(^{15}N)$ = -20 ‰
$\delta_{atm}(^{15}N)$ = -13 ‰
$\delta_{atm}(^{15}N)$ = +5 ‰
lm ($p < 0.05$)
lm ($p > 0.05$)
c_t (Eq. 11 & 12)